*Search for dark matter production in association with a single top quark in proton-proton collisions at √s = 13 TeV*

Published for SISSA by Springer

Received: *March 25, 2025*
Accepted: *August 1, 2025*
Published: *September 17, 2025*

# Search for dark matter production in association with a single top quark in proton-proton collisions at $\sqrt{s} = 13$ TeV

## The CMS collaboration

*E-mail:* cms-publication-committee-chair@cern.ch

Abstract: A search for the production of a single top quark in association with invisible particles is performed using proton-proton collision data collected with the CMS detector at the LHC at $\sqrt{s} = 13$ TeV, corresponding to an integrated luminosity of $138\,\mathrm{fb}^{-1}$. In this search, a flavor-changing neutral current produces a single top quark or antiquark and an invisible state nonresonantly. The invisible state consists of a hypothetical spin-1 particle acting as a new mediator and decaying to two spin-1/2 dark matter candidates. The analysis searches for events in which the top quark or antiquark decays hadronically. No significant excess of events compatible with that signature is observed. Exclusion limits at 95% confidence level are placed on the masses of the spin-1 mediator and the dark matter candidates, and are compared to constraints from the dark matter relic density measurements. In a vector (axial-vector) coupling scenario, masses of the spin-1 mediator are excluded up to 1.85 (1.85) TeV with an expectation of 2.0 (2.0) TeV, whereas masses of the dark matter candidates are excluded up to 0.75 (0.55) TeV with an expectation of 0.85 (0.65) TeV.

Keywords: Beyond Standard Model, Dark Matter, Hadron-Hadron Scattering, Top Physics

ArXiv ePrint: 2503.20033



https://doi.org/10.1007/JHEP09(2025)141

JHEP09(2025)141

## Contents



## 1 Introduction

The standard model (SM) of particle physics is the most complete description of high-energy physics to date. It describes phenomena with unprecedented accuracy, and it has been continuously validated by experimental measurements. Nevertheless, multiple observations have been made that cannot be conclusively explained by the SM, such as invisible mass in the universe inferred from astrophysical [1, 2] and cosmological [3] observations. These observations are consistent with galaxies being predominantly composed of nonrelativistic, weakly interacting mass that has yet to be conclusively explained via beyond-the-SM (BSM) theories. This matter, typically referred to as dark matter (DM), could be produced and observed in a laboratory environment.

A common approach to searching for DM at a collider experiment, such as CMS at the CERN LHC, is an approach known as the "mono-X search strategy". This strategy is based on the assumed interactions of DM with SM particles and the conservation of momentum. If DM is produced in the detector in association with an SM particle X, it creates missing transverse momentum ($p_{\mathrm{T}}^{\mathrm{miss}}$) representing an imbalance of total transverse momentum ($p_{\mathrm{T}}$) in the event. Many searches for DM [4–18] rely on this quantity. Depending on the particle X that is produced in association with the DM, different event signatures appear, e.g., DM in association with a highly energetic light-flavor quark or gluon jet [19, 20], a Z boson [21, 22], a Higgs boson [23, 24], a photon [25, 26], or a single top quark (mono-top) [27, 28].



JHEP09(2025)141

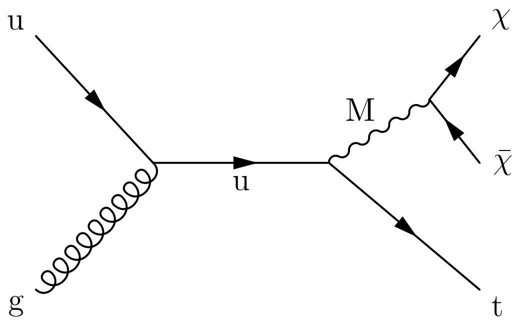


**Figure 1.** Representative Feynman diagram of nonresonant mono-top production at tree level via a flavor-changing neutral current mediated by the spin-1 boson M. The off-shell up quark (u) decays into an on-shell top quark (t) and an M boson. The M boson decays directly to a pair of DM candidates $\chi$ and $\overline{\chi}$.

In this article, a search for DM production in association with a single top quark is presented. The term top quark denotes both the top quark and the top antiquark, and DM production refers to the production of a pair of DM candidates in the GeV to TeV mass range via a mediator particle. The analysis is based on the data set collected by the CMS experiment in proton-proton (pp) collisions at a center-of-mass energy of 13 TeV from 2016 to 2018, corresponding to an integrated luminosity of $138\,\mathrm{fb}^{-1}$.

The mono-top signature consists of a single top quark and a large amount of $p_{\mathrm{T}}^{\mathrm{miss}}$ in the final state. Mono-top production in the SM cannot occur at tree level, but only at one-loop level and at higher orders in quantum chromodynamics (QCD) perturbation theory. Furthermore, Cabibbo suppression [29, 30] as well as the GIM mechanism [31] reduce the cross section for the production of this signature by SM processes. Thus, searches for mono-top production in BSM theories benefit from low expected SM backgrounds. This analysis focuses on the hadronic decay channel of the top quark, $\mathrm{t} \to \mathrm{Wb} \to \mathrm{q\overline{q}'b}$, and targets events in which the top quark obtains a significant recoil against the mediator.

The analysis is optimized for, and results of the search are interpreted in, a simplified model called the nonresonant mono-top model [32]. This simplified model describes the production of two spin-1/2 DM candidates ($\chi$) in association with a top quark by introducing a flavor-changing neutral current (FCNC) process mediated by a new spin-1 boson (M). By extending the SM with this model, nonresonant mono-top production becomes possible at tree level, as shown in figure 1. Because the masses of the new particles are unknown, broad ranges of mediator and DM candidate masses are investigated, and purely vector, as well as purely axial-vector coupling scenarios, are tested.

The event selection is optimized for the mono-top signature. A main event sample enriched in signal events is created by requiring a large-radius jet to capture the top quark, large recoil against the large-radius jet representing the spin-1 boson, and no additional activity in the event. The signal purity is further enhanced by requiring the large-radius jet to be identified as originating from a top quark by a graph neural network [33]. The most important backgrounds in this analysis are events from vector boson production in association with jets (V+jets) and top quark-antiquark pair ($\mathrm{t\overline{t}}$) production. Events from phase space regions not overlapping with the main sample are selected to create control samples enriched in these processes. They are used to constrain the most important background contributions using data.

This article is structured as follows. The CMS detector is described in section 2, and the event and object reconstruction methods are explained in section 3. The signal model is introduced in section 4. The data as well as the signal and background simulations are described in section 5. The event selection is described in section 6 and the methodology of the top quark tagging is covered in section 7. The signal extraction and the background estimation techniques are given in section 8. The systematic uncertainties are detailed in section 9. The analysis results and interpretations are presented in section 10, and the article is summarized in section 11. Tabulated results of this analysis are provided in the HEPData record [34].

## 2 The CMS detector

The central feature of the CMS apparatus is a superconducting solenoid of 6 m internal diameter, providing a magnetic field of 3.8 T. Within the solenoid volume are a silicon pixel and strip tracker, a lead tungstate crystal electromagnetic calorimeter (ECAL), and a brass and scintillator hadron calorimeter (HCAL), each composed of a barrel and two endcap sections. Forward calorimeters extend the pseudorapidity ($\eta$) coverage provided by the barrel and endcap detectors. Muons are measured in gas-ionization detectors embedded in the steel flux-return yoke outside the solenoid. Events of interest are selected using a two-tiered trigger system. The first level (L1), composed of custom hardware processors, uses information from the calorimeters and muon detectors to select events at a rate of around 100 kHz within a fixed latency of about 4 $\mu$s [35]. The second level, known as the high-level trigger, consists of a farm of processors running a version of the full event reconstruction software optimized for fast processing and reduces the event rate to around 1 kHz before data storage [36, 37]. The primary vertex is taken to be the vertex corresponding to the hardest scattering in the event, evaluated using tracking information alone, as described in section 9.4.1 of ref. [38]. A more detailed description of the CMS detector, together with a definition of the coordinate system used and the relevant kinematic variables, can be found in refs. [39, 40].

## 3 Event reconstruction

A particle-flow algorithm [41] aims to reconstruct and identify each individual particle in an event, with an optimized combination of information from the various elements of the CMS detector. The energy of photons is obtained from the ECAL measurement. The energy of electrons is determined from a combination of the electron momentum at the primary vertex, as determined by the tracker, the energy of the corresponding ECAL cluster, and the energy sum of all bremsstrahlung photons spatially compatible with originating from the electron track. The momentum of muons is measured in the inner tracker and the muon chambers. The energy of charged hadrons is determined from a combination of their momentum measured in the tracker and the matching ECAL and HCAL energy deposits, corrected for the response function of the calorimeters to hadronic showers. Finally, the energy of neutral hadrons is obtained from the corresponding corrected ECAL and HCAL energies.



JHEP09(2025)141

For each event, hadronic jets are clustered from these reconstructed particles using the infrared- and collinear-safe anti-$k_\mathrm{T}$ algorithm [42, 43] with a distance parameter of 0.4 or 1.5, referred to as AK4 and AK15 jets, respectively. Jet momentum is determined as the vectorial sum of all particle momenta in the jet, and is found from simulation to be, on average, within 5 to 10% of the true momentum over the entire range and detector acceptance. Additional pp interactions within the same or nearby bunch crossings (pileup) can contribute additional tracks and calorimetric energy depositions to the jet momentum. To mitigate this effect for AK4 jets, charged particles identified to be originating from pileup vertices are discarded and an offset correction is applied to adjust for remaining contributions [44]. AK15 jets have a larger area and are more sensitive to the effects of pileup. For this reason, the pileup-per-particle identification algorithm [44, 45] is used to mitigate the effect of pileup for AK15 jets at the reconstructed-particle level, making use of local shape information, event pileup properties, and tracking information.

Jet energy corrections are derived from simulation studies so that the average measured energy of jets becomes identical to that of generated-particle level jets. In situ measurements of the momentum balance in $\gamma$+jets, Z+jets events, as well as events composed uniquely of jets produced through the strong interaction (QCD multijet events), are used to account for any residual differences in the jet energy scale between data and simulation [46]. For jets with central $|\eta|$, the jet energy resolution ranges from around 15% at 30 GeV, to 10% at 100 GeV, and 5% at 1 TeV [46]. Additional selection criteria are applied to each jet to remove jets that are potentially dominated by anomalous contributions from various sub-detector components or reconstruction failures [47].

For electrons, photons, and muons, a loose and a tight selection is established. Loose objects are selected with a high identification efficiency and are used to veto events with additional objects in the final state. Tight objects are selected with a lower misidentification rate compared to the loose selection. They are used to select dedicated event samples, enriched with events from electroweak (EW) processes and $\mathrm{t\bar{t}}$ production with prompt electrons, muons, and photons in the final state. The tight collections are always subsets of the corresponding loose collections.

Tight (loose) electrons must fulfill $p_\mathrm{T} > 40$ (10) GeV and $|\eta| < 2.4$ (2.5). A sequence of additional selection criteria is applied to improve the correct identification of genuine electrons, with an efficiency of around 70 (95)% for tight (loose) electrons [48]. Tight (loose) photons must fulfill $p_\mathrm{T} > 200$ (20) GeV and $|\eta| < 1.479$ (2.5). In the 2016 data-taking period, the $p_\mathrm{T}$ threshold for selecting tight photons is increased to $p_\mathrm{T} > 230$ GeV. Additional requirements are imposed in order to improve the identification of genuine photons, which lead to an identification efficiency of 80 (90)% for tight (loose) photons [48].

Tight (loose) muons must fulfill $p_\mathrm{T} > 30$ (20) GeV and $|\eta| < 2.4$. In the 2018 data-taking period, the $p_\mathrm{T}$ threshold for selecting loose muons is lowered to $p_\mathrm{T} > 15$ GeV, while all other selection criteria stay the same. The isolation variable

$$I^{\mu}_{\mathrm{rel}} = \frac{1}{p^{\mu}_\mathrm{T}} \left[\sum p_\mathrm{T}^{\mathrm{charged}} + \max\left(0, \sum p_\mathrm{T}^{\mathrm{neutral}} + \sum p_\mathrm{T}^{\gamma} - p_\mathrm{T}^{\mathrm{pileup}}\right)\right] \tag{3.1}$$

is employed to increase the selection purity of prompt muons produced in the hard process.



JHEP09(2025)141

| | $p_T$ greater than | $\lvert\eta\rvert$ less than | ID efficiency | $I^{\mu}_{\text{rel}}$ less than |
|---|---|---|---|---|
| Loose electrons | 10 GeV | 2.5 | 95% | — |
| Tight electrons | 40 GeV | 2.4 | 70% | — |
| Loose photons | 20 GeV | 2.5 | 90% | — |
| Tight photons | 230 GeV (2016), 200 GeV (2017, 2018) | 1.479 | 80% | — |
| Loose muons | 10 GeV | 2.4 | 99.8% | 0.25 |
| Tight muons | 20 GeV (2016, 2017), 15 GeV (2018) | 2.4 | 96.0% | 0.15 |

**Table 1.** Requirements on electrons, photons, and muons that pass the loose or tight selection. For all objects, the minimal $p_T$, the maximal $|\eta|$, and the efficiency of the object identification (ID) are provided. For muons, the requirements on the relative isolation $I^{\mu}_{\text{rel}}$ are also listed. A more detailed discussion is given in the text.

The scalar $p_T$ sums of charged particles, neutral hadrons, and photons, denoted as $\sum p_T^{\text{charged}}$, $\sum p_T^{\text{neutral}}$, and $\sum p_T^{\gamma}$, respectively, are calculated for reconstructed particle candidates in a cone of radius $\Delta R = \sqrt{(\Delta\eta)^2 + (\Delta\phi)^2} < 0.4$ around the muon. Here, $\Delta\eta$ and $\Delta\phi$ correspond to the difference in $\eta$ and in the azimuthal angle $\phi$ (measured in radians) between the muon and a reconstructed particle candidate. The muon transverse momentum $p_T^{\mu}$ is excluded from these calculations. The estimated contribution from pileup ($p_T^{\text{pileup}}$) is subtracted from $\sum p_T^{\text{neutral}} + p_T^{\gamma}$. Tight (loose) muons must fulfill $I^{\mu}_{\text{rel}} < 0.15$ (0.25). The muon identification has an efficiency of 96.0 (99.8)% for tight (loose) muons [49].

The most important selection criteria for electrons, photons, and muons in this analysis are summarized in table 1.

The missing transverse momentum vector $\vec{p}_T^{\text{miss}}$ is computed as the negative vector sum of the transverse momenta of all the particle-flow candidates, in an event, including electrons, muons, photons, and charged and neutral hadrons. Its magnitude is denoted as $p_T^{\text{miss}}$ [47]. The $\vec{p}_T^{\text{miss}}$ is modified to account for corrections to the energy scale of the reconstructed jets in the event.

The hadronic recoil $\vec{R}_T$ represents the recoil against the hadronic activity in the transverse plane of the event. In this analysis, the hadronic recoil is defined as

$$\vec{R}_T = \vec{p}_T^{\text{miss}} + \sum_i \vec{p}_{T,i}, \tag{3.2}$$

where the sum runs over all electrons, muons and photons in the event, which pass the loose selections. Its magnitude is denoted as $R_T$.

The quantity $p_T^{\text{miss, no }\mu}$ is used in the trigger and is computed using the same method as for $p_T^{\text{miss}}$, but excluding muon candidates in the trigger reconstruction from the calculation. If no other electrons or photons are present in the final state, $p_T^{\text{miss, no }\mu}$ is very similar to the hadronic recoil. A trigger that selects events based on $p_{\mathrm{T}}^{\text{miss, no }\mu}$ directly targets the phase space of the search in the signal region (SR) and some of the control regions (CRs) defined in section 6.

Light flavor quarks (u, d, s) and gluons produced in the primary vertex fragment and deposit clusters of energy in the ECAL and HCAL. However, bottom (b) quarks form semi-stable mesons that travel a finite distance before they decay. The DeepJet tagger [50] is used to select jets that are consistent with a b quark at a working point corresponding to a 10% mistagging probability of light-flavor jets. The efficiency to identify jets originating from a b quark is approximately 90% at this working point. The selection efficiency and mistag rate of the DeepJet tagger in simulation are corrected with scale factors measured in data to account for residual differences between data and simulation [50].

In the signal topology, the top quark (t) recoils off the DM candidates in the event. This causes the top quark to have a significant boost that allows for its decay products to be clustered into a single large-radius jet. A graph neural network approach (ParticleNet) [33] is used to assign probability-like scores to the possible origins (top quark, Higgs boson, EW bosons, QCD multijet) of large-radius jets. The output of ParticleNet is used to select events in which the large-radius jet likely originated from a hadronically decaying top quark.

## 4 Signal model

The analysis searches for a single top quark produced via an FCNC process. The top quark is produced in association with a spin-1 boson that has FCNC couplings to quarks and can decay directly into DM candidates. Figure 1 depicts a representative Feynman diagram of this process. This production channel is also called nonresonant mono-top production.

The effective Lagrangian allowing nonresonant mono-top production at tree level in the simplified model [32] studied in this paper is given by

$$\begin{aligned}\mathcal{L} = \mathcal{L}_{\mathrm{SM}} &+ \underbrace{\mathrm{M}_\mu \overline{U}(g_{\mathrm{v}}^U \gamma^\mu + g_{\mathrm{a}}^U \gamma^\mu \gamma_5) U}_{\text{FCNC up-type e.g. u}\to\text{t}} + \underbrace{\mathrm{M}_\mu \overline{D}(g_{\mathrm{v}}^D \gamma^\mu + g_{\mathrm{a}}^D \gamma^\mu \gamma_5) D}_{\text{FCNC down-type e.g. d}\to\text{b}} \\ &+ \underbrace{\mathrm{M}_\mu \overline{\chi}(g_{\mathrm{v}}^\chi \gamma^\mu + g_{\mathrm{a}}^\chi \gamma^\mu \gamma_5) \chi}_{\text{decay M}\to\chi\overline{\chi}} + \mathcal{L}_{\text{kin, mass, gauge}}(\mathrm{M}_\mu, m_{\mathrm{M}}, \chi, m_\chi).\end{aligned} \tag{4.1}$$

The SM Lagrangian $\mathcal{L}_{\mathrm{SM}}$ is extended by the mass, kinetic, and gauge terms of the newly introduced fields, as well as a term describing the interactions between the spin-1 mediator M with mass $m_{\mathrm{M}}$ and SM quarks or the DM candidates $\chi$ with mass $m_\chi$. The $\chi$ is assumed to be stable and the width of the mediator is dependent on the $m_{\mathrm{M}}$, $m_\chi$, and the axial and axial-vector couplings as defined in [51]. Here, $U$ represents the up-type quarks $(\mathrm{u}, \mathrm{c}, \mathrm{t})^T$ and $D$ the down-type quarks $(\mathrm{d}, \mathrm{s}, \mathrm{b})^T$ with the color indices implied, $g_{\mathrm{v}}^\chi$ ($g_{\mathrm{a}}^\chi$) is the vector (axial-vector) coupling to DM candidates, and $g_{\mathrm{v}}^U$, $g_{\mathrm{a}}^U$, $g_{\mathrm{v}}^D$, $g_{\mathrm{a}}^D$ are called flavor matrices, parameterizing the interaction strength of the different up/down-type quarks with the M boson. The subscripts "v" and "a" represent the vector and axial-vector couplings. The diagonal and nondiagonal elements of the flavor matrices represent the interaction strengths between up-type and down-type quarks of the same and different flavor, respectively. Depending on which elements of the flavor matrices are chosen as nonzero, different mono-X signatures can appear.

The mono-top model described here is specified such that an FCNC connects the up-type quarks of the first and third generations, allowing mono-top production at tree level. This implies that only $(g^U_{\mathrm{v/a}})_{13} \neq 0$, whereas all other coupling elements of the up-type flavor matrices are set to zero. This is motivated by the fact that top quark production through an $s$-channel up quark is favored by parton distribution functions (PDFs) at the LHC. For SM gauge invariance, the same-generation down-type couplings need to be similar to the up-type couplings. This means that also $(g^D_{\mathrm{v/a}})_{13} \neq 0$, whereas all other coupling elements of the down-type flavor matrices are set to zero.

For the nominal coupling scenario of this analysis, i.e., a vector-only coupling scenario, all axial-vector couplings are set to zero, and $(g^U_{\mathrm{v}})_{13} = 0.25$ and $g^\chi_{\mathrm{v}} = 1$ is chosen, following the recommendations of the LHC Dark Matter working group [52]. Larger values of $(g^U_{\mathrm{v}})_{13}$ enhance decays of the mediator into bottom or down quarks, which are also kinematically favored. This would suppress the branching fraction of the mediator's decay into DM candidates. An alternative axial-vector coupling scenario, for which all vector couplings are set to zero and $(g^U_{\mathrm{v}})_{13} = 0.25$ and $g^\chi_{\mathrm{a}} = 1$ is chosen, is also considered.

## 5 Data and simulated samples

The data set used in the analysis was collected with the CMS experiment in pp collisions in 2016, 2017, and 2018 and corresponds to a total integrated luminosity of 138 fb$^{-1}$ at a center-of-mass energy of 13 TeV.

Signal and background events are simulated at leading order (LO) with PYTHIA (v. 8.240) [53], or at next-to-LO (NLO) in perturbative QCD with MADGRAPH5_aMC@NLO (v. 2.6.5) [54] or POWHEG (v. 2) [55–57], depending on the process, as defined below. The NNPDF (v. 3.1) PDFs [58] at next-to-NLO (NNLO) are used for all processes. All generated events are interfaced with PYTHIA (v. 8.240) with the CP5 tune [59] to generate the parton shower and to model the hadronization. A detailed simulation of the response of the CMS detector is performed with GEANT4 [60] for each event. For all simulations, the value of the top quark mass is set to 172.5 GeV.

The signal is simulated at NLO QCD perturbation theory using MADGRAPH5_aMC@NLO [54] based on the nominal coupling scenario described in section 4. The implementation of the model [61] is provided by the authors of ref. [32]. Alternative coupling scenarios are realized via a reweighting procedure in MADGRAPH5_aMC@NLO [62]. Signal samples in the range of mediator mass $200 \leq m_{\mathrm{M}} \leq 2500$ GeV and DM candidate mass $50 \leq m_\chi \leq 1500$ GeV have been produced to account for the unknown masses of the newly introduced particles. Only on-shell decays of the mediator into DM candidates are considered, i.e., the relation $2m_\chi \leq m_{\mathrm{M}}$ must be fulfilled for a mass hypothesis to be taken into account. The lower threshold on the mediator mass is chosen such that the mediator mass is always greater than the mass of the top quark to avoid new decay channels of the top quark mediated by the M boson.

The $\mathrm{t\bar{t}}$ background process is simulated using POWHEG at NLO accuracy in the five-flavor scheme [63]. The total cross section is normalized to calculations at NNLO precision in QCD including soft gluon resummation of next-to-next-to-leading logarithmic terms, obtained with TOP++ (v. 2.0) [64–70].

Backgrounds from single top quark (single t) production in the $t$ channel, and in association with a W boson (tW), are simulated with POWHEG [71, 72]. Single t production in the $s$ channel is simulated with MadGraph5_aMC@NLO. The inclusive production cross sections are normalized to NLO calculations for single t production in the $t$ and $s$ channels [73, 74], and to approximate NNLO calculations for tW production [75].

Further background contributions arise from V+jets production where the boson V represents a W, Z, or $\gamma$ boson. They are simulated with MadGraph5_aMC@NLO at NLO QCD precision with up to two additional partons in the final state, where the matching of matrix-element jets with those from parton showers is performed using the FxFx [76] prescription. The $\gamma$+jets process is generated at NLO accuracy in perturbative QCD with up to one parton in the matrix element calculation. A reweighting procedure based on the vector boson $p_{\mathrm{T}}$ is used in order to apply EW corrections at NLO precision, following ref. [77]. This improves the SM background prediction in phase space regions where contributions from V+jets production are dominant. These EW corrections become relevant when the vector boson has a large transverse momentum.

Additional minor background contributions arise from diboson (WW, WZ, and ZZ) as well as QCD multijet production. These are simulated at LO using the PYTHIA event generator. The WW and ZZ processes are normalized to the NNLO cross sections [78, 79] and the WZ process is scaled to the NLO calculation [80]. QCD multijet production is scaled to the LO cross section extracted from the generated event sample.

## 6 Event selection

The selection targets events with a significant amount of $R_{\mathrm{T}}$. The selected events are subsequently divided into SRs with a high selection efficiency for the signal, and CRs, which are depleted of signal and enriched in background processes. The CRs target processes equal or similar to the most important backgrounds in the SR. They take an important role in the background estimation of the $\mathrm{Z}(\nu\nu)$+jets and $\mathrm{t\bar{t}}$ processes, which is further explained in section 8. To estimate the $\mathrm{Z}(\nu\nu)$+jets shape in the SR, the method exploits the similarity of this process to $\mathrm{Z}(\ell\ell)$+jets, $\mathrm{W}(\ell\nu)$+jets, and $\gamma$+jets production.

Three triggers are used to select events in this analysis. A trigger that is activated on events with a large amount of $p_{\mathrm{T}}^{\text{miss, no }\mu}$ is used to collect events in the SRs and in CRs of background processes with muons in the final state. In order to collect events in the CRs of background processes with electrons (photons) in the final state, an electron (a photon) trigger is used.

The signal events contain a hadronically decaying top quark and large $p_{\mathrm{T}}^{\text{miss}}$. As a phase space with top quarks with a high Lorentz boost is targeted, the decay products of the top quark can be reconstructed in a single AK15 jet. Events considered in this analysis must fulfill $R_{\mathrm{T}} > 350\,\mathrm{GeV}$. This selection on $R_{\mathrm{T}}$ ensures that the analysis selects events in which the $p_{\mathrm{T}}^{\text{miss, no }\mu}$ trigger efficiency is significantly greater than 95% and removes events with low $R_{\mathrm{T}}$ that typically have a worse signal-to-background ratio. Events must have at least one large-radius AK15 jet with $p_{\mathrm{T}} > 250\,\mathrm{GeV}$ and $|\eta| < 2.4$. The leading AK15 jet, i.e., the AK15 jet with the highest $p_{\mathrm{T}}$ in the event, and the $\vec{R}_{\mathrm{T}}$ must fulfill $|\Delta\phi| > 1.5$. The AK4 jets that are considered in this analysis are required to have $p_{\mathrm{T}} > 30\,\mathrm{GeV}$, $|\eta| < 2.4$, and to not originate from detector noise. They are mainly used to identify b jets outside the leading AK15 jet in the event. For events to be further considered, all AK4 jets, including those which overlap with the leading AK15 jet, must have a $\Delta\phi$ separation from the $\vec{R}_{\mathrm{T}}$ by at least 0.5 radians. This requirement heavily reduces contributions from QCD multijet production in which the $p_{\mathrm{T}}^{\mathrm{miss}}$ is typically mismeasured collinearly with one of the leading AK4 jets.

In a large fraction of the 2018 data-taking period, two HCAL endcap modules (HEM) were not functioning, thereby impacting the jet energy measurements in the affected detector regions. In order to account for this HEM effect, events are vetoed if any AK4 jet fulfilling a very loose set of selections is found in the corresponding detector regions $-1.57 < \phi < -0.87$ and $-3.0 < \eta < -1.3$. To further reduce events in which a jet is fully lost due to the HEM issue, contributing at low values of $p_{\mathrm{T}}^{\mathrm{miss}}$, events are vetoed if $p_{\mathrm{T}}^{\mathrm{miss}} < 470\,\mathrm{GeV}$ and $-1.62 < \phi(\vec{p}_{\mathrm{T}}^{\mathrm{miss}}) < -0.62$, following ref. [19].

In this analysis, only AK4 jets that are well separated from the leading AK15 jet in the event are considered for b tagging. The purpose of these b-tagged jets is to either veto or explicitly allow for additional b quarks in the event, which do not originate from the decay of the boosted top quark. To consider an AK4 jet as b tagged in this analysis, it must have a $\Delta R$ distance of more than 1.5 from the leading AK15 jet and it must fulfill the requirements of the loose working point of the DeepJet tagger [50] corresponding to a mistagging probability of light-flavor quark and gluon jets of approximately 10%.

Events that fulfill the preselection and have passed the $p_{\mathrm{T}}^{\text{miss, no }\mu}$, the electron, or the photon triggers are further categorized. An SR is formed in order to create an event sample with a high selection efficiency on signal events and a high rejection rate of events from reducible background processes, e.g., $\mathrm{W}(\ell\nu)$+jets and $\mathrm{t\bar{t}}$ production. In addition, different CRs are created, which are enriched in events from specific background processes. The different CRs target $\mathrm{Z}(\ell\ell)$+jets, $\mathrm{W}(\ell\nu)$+jets, $\gamma$+jets, and $\mathrm{t\bar{t}}(\ell\nu)$ production. The SR and CRs are mutually exclusive, i.e., each selected event is uniquely assigned to a single analysis region.

For the SR, a data set collected with the $p_{\mathrm{T}}^{\text{miss, no }\mu}$ trigger is used. Events in the SR must not contain any electrons, muons, or photons from the loose collections, as well as any b-tagged jet.

The CRs enriched in events from $\mathrm{Z}(\ell\ell)$+jets, $\mathrm{W}(\ell\nu)$+jets, and $\mathrm{t\bar{t}}$ production are formed by selecting events with leptons in the final state. For each of these leptonic CRs, two versions exist: one with electrons and one with muons in the final state. In the CRs with electrons in the final state, events must have activated the single electron trigger, while in CRs with muons in the final state, events must have activated the $p_{\mathrm{T}}^{\text{miss, no }\mu}$ trigger. In these CRs, $p_{\mathrm{T}}^{\text{miss, no }\mu}$ corresponds to the definition of $R_{\mathrm{T}}$ in section 3, which motivates the use of the $p_{\mathrm{T}}^{\text{miss, no }\mu}$ trigger. In addition, a CR enriched in prompt $\gamma$ production is formed by selecting events with a photon in the final state from the photon-triggered data set.

Events in the $\mathrm{Z}(\ell\ell)$ CR require exactly two same-flavor leptons with an invariant mass of the two-lepton system $m_{\ell\ell}$ near that of the nominal Z boson mass [81], i.e., $60 < m_{\ell\ell} < 120\,\mathrm{GeV}$, and low $p_{\mathrm{T}}^{\mathrm{miss}}$. The requirements on well-reconstructed electrons and muons are slightly relaxed in the $\mathrm{Z}(\ell\ell)$ CR, i.e., the loose electron and muon collections are used for event selection, to mitigate the low branching fractions of the Z boson decay into charged leptons. In the $\mathrm{W}(\ell\nu)$ CR, a single tight lepton, significant $p_{\mathrm{T}}^{\mathrm{miss}}$, and no additional b-tagged



JHEP09(2025)141

| Observable | SR | $Z(\ell\ell)$ | $W(\ell\nu)$ | $t\bar{t}(\ell\nu)$ | $\gamma$ |
|---|---|---|---|---|---|
| $R_T$ | | | $> 350$ GeV | | |
| Leading AK15 jet $p_T$ | | | $> 250$ GeV | | |
| $\Delta\phi(\text{AK15 jet}, \vec{R}_T)$ | | | $> 1.5$ | | |
| $\min \Delta\phi(\text{AK4 jet}, \vec{R}_T)$ | | | $> 0.5$ | | |
| Additional objects | — | 2 $\ell$ (both loose) | 1 $\ell$ | 1 $\ell$ | 1 $\gamma$ |
| b-tagged AK4 jets | 0 | — | 0 | $\geq 1$ | 0 |
| $p_T^{miss}$ | — | $< 120$ GeV | $> 150$ GeV | $> 150$ GeV | — |
| $m_{T,W}$ | — | — | $< 150$ GeV | $< 150$ GeV | — |
| $m_{\ell\ell}$ | — | $60 < m_{\ell\ell} < 120$ GeV | — | — | — |

**Table 2.** Overview of the selections for the SR and the CRs, including the preselection. In the $Z(\ell\ell)$ CRs, loose leptons are used for the selection of additional objects in the final state. In all other CRs, leptons and photons from the tight collections are used to determine the number of additional objects. CRs with final state leptons are defined separately for electrons and muons. The first four selections are common to the SR and all CRs.

jets in the event are required. Except for the requirement of at least one additional b-tagged jet in the event, the selection criteria of the $t\bar{t}(\ell\nu)$ CR are the same as those of the $W(\ell\nu)$ CR. Events in the $\gamma$ CR require one isolated photon and no additional b-tagged jets. If an event passes all selections, but contains additional loose electrons, muons, or photons compared to the aforementioned selections, it is removed from the analysis data set.

In the $t\bar{t}(\ell\nu)$ and $W(\ell\nu)$ CRs, an additional requirement on the transverse mass of the W boson, defined as

$$m_{T,W} = \sqrt{2p_{T,\ell}p_T^{miss}[1 - \cos\Delta\phi(\ell, \vec{p}_T^{miss})]}, \tag{6.1}$$

is introduced to ensure an orthogonal selection to a potential mono-top search in the leptonic top quark decay channel with the same data set. Here, $\Delta\phi(\ell, \vec{p}_T^{miss})$ is the azimuthal difference between the selected tight lepton (electron or muon) $\ell$ and $\vec{p}_T^{miss}$. Since mono-top signatures with a leptonic top quark decay lead to values of $m_{T,W}$ well above the W boson mass, events in the $t\bar{t}(\ell\nu)$ and $W(\ell\nu)$ CRs are required to fulfill $m_{T,W} < 150$ GeV.

A summary of the selections can be found in table 2.

The distribution of the magnitude of $R_T$ in the SR before the simultaneous binned maximum likelihood fit (prefit) is given in figure 2. All background distributions are extracted from simulation, and all corrections and uncertainties, mentioned in section 9, are applied. As $R_T$ represents the recoil against the top quark in the event, it is a measure for the mediator $p_T$ in the signal process. It is clearly visible that the mono-top signal tends to have larger $R_T$ values than the expected background. The most important background processes are $Z(\nu\nu)$+jets and $W(\ell\nu)$+jets production, in which the lepton from the W boson decay is either out of acceptance, not reconstructed, or not identified. Both the SR and CRs will use top quark tagging, as detailed in section 7, to increase the sensitivity to the signal process and to improve the modeling of important SM backgrounds.



JHEP09(2025)141

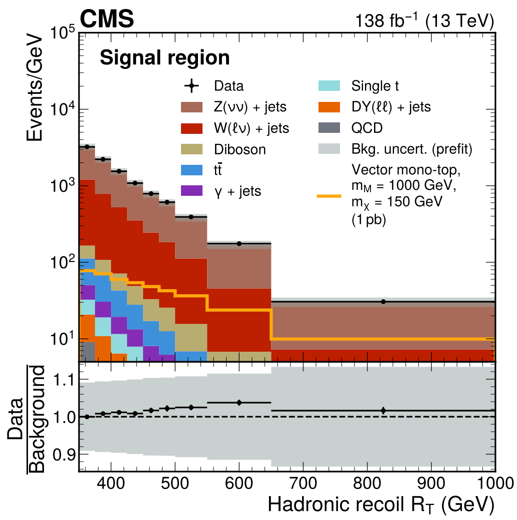


**Figure 2.** Prefit distribution of the magnitude of the hadronic recoil $R_\mathrm{T}$ in the SR. The last bin of the distribution also contains events with $R_\mathrm{T} > 1000\,\mathrm{GeV}$. The distributions of background processes from simulation are stacked together. All nominal corrections are applied to the simulated SM processes. A representative mono-top signal (vector coupling scenario) with a mediator mass of 1 TeV, a DM candidate mass of 150 GeV, and a cross section of 1 pb is overlaid as an orange line. The gray band represents the statistical and unconstrained systematic uncertainties in the simulated event yields.

## 7 Top quark tagging

For the V+jets background processes, the large-radius jet originates from QCD radiation processes, while for the signal process it is mostly produced in the decay of the top quark. This property is exploited to reduce the contributions of the V+jets background processes to the SR.

For AK15 jets, a discriminator (top quark tagger, t tagger), based on the graph neural network ParticleNet, is employed to distinguish jets originating from the hadronic decay of a top quark from jets due to QCD radiation. This discriminator provides probability-like scores $p_P$ for an AK15 jet to stem from a certain physics process $P$, e.g., from a hadronic top quark decay ($p_\mathrm{t}$), from pure QCD radiation ($p_\mathrm{QCD}$), or from other possible origins that are not relevant for this analysis. As discriminant, the aggregated score

$$p_{\mathrm{t/QCD}} = \frac{p_\mathrm{t}}{p_\mathrm{t} + p_\mathrm{QCD}} \tag{7.1}$$

is used, which expresses the probability that the AK15 jet originates from a hadronic top quark decay as opposed to the hypothesis that the jet is purely QCD-initiated.

A requirement on the minimal value of the discriminant in eq. (7.1) is used to tag the leading AK15 jet as a t jet or as a QCD jet. The working point is chosen such that the misidentification rate of QCD jets being tagged as t jets is 1% in simulated $Z(\nu\nu)$+jets events. In the SR and each CR, the t tagging of the leading AK15 jet is used to split events into two samples, according to whether the leading AK15 jet in the event is tagged as a t jet (t-pass) or not (t-fail). An overview of all analysis categories after applying the t tagging requirement is given in figure 3. It should be noted that a t-pass and t-fail category are



JHEP09(2025)141

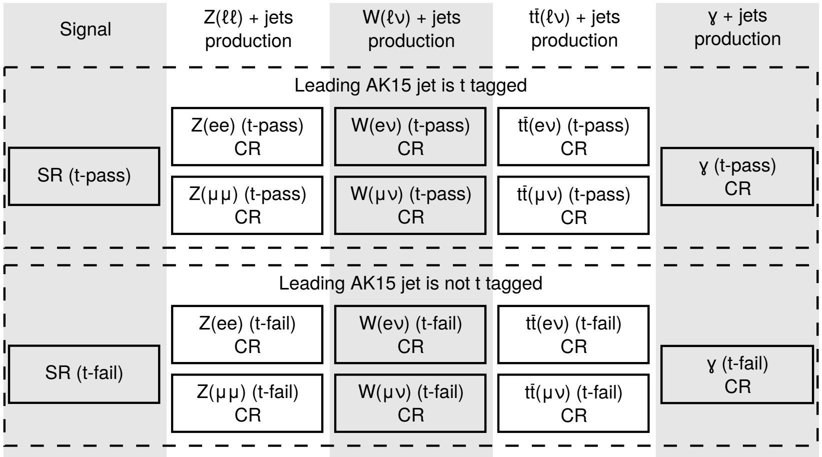


**Figure 3.** Categorization of events into SRs and CRs, which are sensitive to specific processes, namely the mono-top signal, V+jets ($\mathrm{V} = \mathrm{Z}, \mathrm{W}, \gamma$) processes, and $\mathrm{t\bar{t}}$ production. Each column contains categories that target the same process. For CRs with leptons in the final state, a version with electrons and a version with muons in the final states exist. Finally, in each category a split is performed based on whether the leading AK15 jet is t tagged or not.

created for all SRs and CRs introduced in section 6. The SR (t-fail) category is not sensitive to signal, but is used as a closure test for the modeling of SM processes.

The discriminator is operated at a working point where the t quark identification efficiency in simulation varies from 45 to 80% for AK15 jets that pass the t tagging working point, depending on the AK15 jet $p_{\mathrm{T}}$. Top quark jets with higher $p_{\mathrm{T}}$ exhibit higher tagging efficiencies. The inclusive t tagging efficiency is approximately 67%. At this working point, the misidentification probability for AK15 jets of the QCD jet (b jet) class is 1–2 (8–12)% in simulation, depending on the AK15 jet $p_{\mathrm{T}}$.

The t tagging efficiency and misidentification rates are measured using three aggregated AK15 jet classes in the $\mathrm{t\bar{t}}(\ell\nu)$ and $\gamma$ CRs, respectively. The jet classes are defined in simulation based on the number of quarks from the top quark decay that are matched within the AK15 jet cone, and whether there is b flavor within the jet via ghost-hadron matching [82]. An AK15 jet that has at least two quarks from the hadronic top quark decay within its jet radius is defined as belonging to the t jet class. If an AK15 jet has at least one ghost hadron with b flavor, which has been clustered into the reconstructed jet, but it does not fulfill the requirements of the t jet class, it is assigned to the b jet class. AK15 jets that do not meet the requirements of either the t jet nor the b jet class form the QCD jet class.

The $\mathrm{t\bar{t}}(\ell\nu)$ CRs represent an environment in which a large fraction of t-tagged jets originates from a hadronic top quark decay. The t tagging efficiency is measured in a combined $\mathrm{t\bar{t}}(\ell\nu)$ CR, which is merged from the $\mathrm{t\bar{t}}(\mathrm{e}\nu)$ and $\mathrm{t\bar{t}}(\mu\nu)$ CRs, defined in section 6. The t tagging efficiency in simulation is calculated by determining the fraction of AK15 jets in the t jet class, which are also t tagged. In data, the number of all (t-tagged) AK15 jets in the t class is estimated by subtracting the number of all (t-tagged) AK15 jets from the b jet and QCD jet classes, both obtained from simulation. The ratio of the t-tagged AK15 jets to the total number of AK15 jets from the t jet class is the efficiency of correctly identifying t jets. The misidentification rate of t tagged AK15 jets that originate from QCD processes is determined in a similar manner in the $\gamma$ CRs. The t tagging efficiency and the QCD misidentification rate are measured as functions of the leading AK15 jet $p_{\mathrm{T}}$. To correct for residual differences of the t tagging efficiency and the misidentification rate in data and simulation, the ratio of the efficiencies is used as a scale factor. It is applied to simulation as a per-event weight based on the properties of the leading AK15 jet. The t tagging scale factor between data and simulation ranges between 0.6 and 1, where 1 is equivalent to the behavior of the t tagging in simulation being perfectly consistent with that on data. Variations associated with systematic uncertainties from section 9 are propagated to the measurement of the scale factors.

In simulation, around 5% of the leading AK15 jets in the $\gamma$ CR, and around 10% of the leading AK15 jets in the $\mathrm{t\bar{t}}(\ell\nu)$ CRs, are assigned to the b jet class. Additionally, in the t-pass SR, approximately 50% of the t-tagged AK15 jets originate from QCD production. The second-largest fraction (25–35%) arises from top quark-initiated jets. Mistagged b jets constitute the third-largest group, with 15–20% of the t-tagged jets originating from bottom quarks. No misidentification rate is measured in data for these cases. The ratio of the efficiencies in data and simulation is assumed to be unity, and a 50% uncertainty is assigned to this ratio. This uncertainty is also propagated to the t tagging and QCD misidentification rate measurements as a systematic uncertainty.

For the SR (t-pass) and the SR (t-fail), the resulting distributions of the hadronic recoil after applying the split according to the t tagging discriminant are shown in figure 4. All background distributions are extracted from simulation. The SR (t-pass) region is enriched with signal events as well as background events containing hadronically decaying top quarks, e.g., $\mathrm{t\bar{t}}$ events. However, $\mathrm{Z}(\nu\nu)$+jets and $\mathrm{W}(\ell\nu)$+jets events still are the largest background contribution because of their large cross sections, limited detector efficiency, and misidentification of purely QCD-initiated jets as top jets. The SR (t-fail) region almost completely consists of $\mathrm{Z}(\nu\nu)$+jets and $\mathrm{W}(\ell\nu)$+jets events. It is mainly used to constrain systematic uncertainties related to the aforementioned processes together with the other CRs of the analysis.

## 8 Background estimation and signal extraction

The signal is extracted with a binned maximum likelihood fit of the predicted backgrounds and the signal model to the $R_{\mathrm{T}}$ distribution in data. All SRs and CRs, i.e., all analysis regions that are depicted in figure 3, and all data-taking periods are combined in the fit. Systematic uncertainties are parameterized by nuisance parameters. The statistical analysis is carried out with Combine [83] based on the RooFit [84] and RooStats [85] software packages.

The $\mathrm{Z}(\nu\nu)$+jets production constitutes the largest background contribution in the SR. In order to constrain its yield and the shape of its $R_{\mathrm{T}}$ distribution as much as possible, data in CRs are used. However, it is not possible to create a $\mathrm{Z}(\nu\nu)$+jets CR for events with large $R_{\mathrm{T}}$ and a high-$p_{\mathrm{T}}$, t-tagged AK15 jet as there is no additional event activity to separate these events from the SR. Instead, processes similar to $\mathrm{Z}(\nu\nu)$+jets, for which dedicated CRs can be constructed, such as W+jets, Z+jets, and $\gamma$+jets, are used for this purpose. In these processes, events with a vector boson or photon, as well as a high-$p_{\mathrm{T}}$ AK15 jet are produced in the phase space considered in this analysis, similar to $\mathrm{Z}(\nu\nu)$+jets.



JHEP09(2025)141

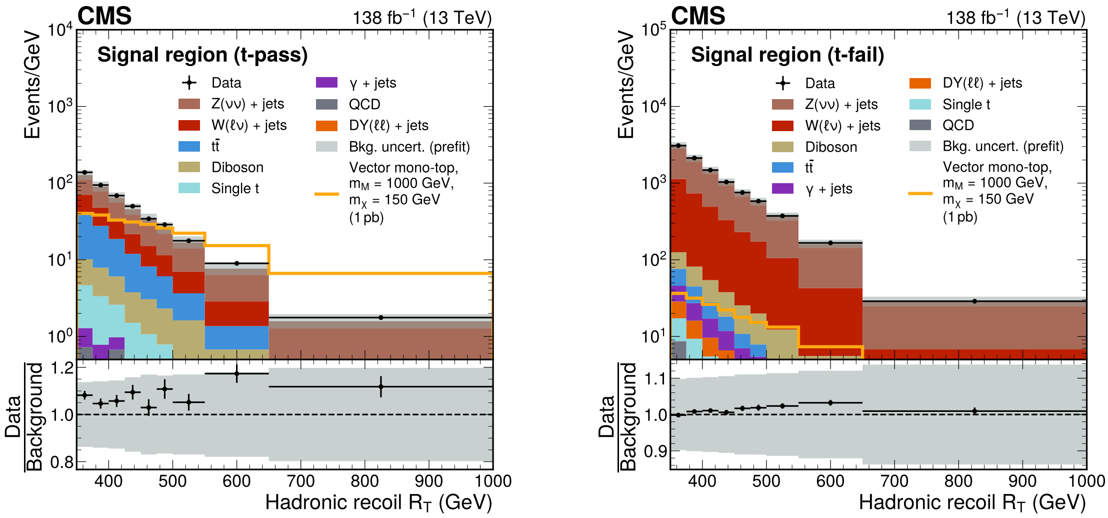


**Figure 4.** Prefit distributions of the magnitude of the hadronic recoil $R_\mathrm{T}$ in the SR (t-pass) and SR (t-fail). The last bin of each distribution also contains events with $R_\mathrm{T} > 1000\,\mathrm{GeV}$. The distributions of background processes from simulation are stacked together. All nominal corrections are applied to the simulated SM processes. A representative mono-top signal (vector coupling scenario) with a mediator mass of 1 TeV, a DM candidate mass of 150 GeV, and a cross section of 1 pb is overlaid as an orange line. The gray band represents the statistical and unconstrained systematic uncertainties in the simulated event yields.

The estimation of Z$(\nu\nu)$+jets production in the SR is directly implemented into the formalism of the maximum likelihood fit. The same method has previously been used in [27]. In each bin of the $R_\mathrm{T}$ distribution, the Z$(\nu\nu)$+jets bin yield in the SR is estimated as freely floating parameter $r^{\mathrm{Z}(\nu\nu)}$ in the fit. In order to constrain $r^{\mathrm{Z}(\nu\nu)}$, other V+jets process contributions in analysis regions of this search are expressed as the product $t_{\mathrm{V+jets}} r^{\mathrm{Z}(\nu\nu)}$ of a transfer factor (TF) and $r^{\mathrm{Z}(\nu\nu)}$. The TFs

$$t_{\mathrm{V+jets}} = \frac{n^{\mathrm{sim}}_{\mathrm{V+jets}}}{n^{\mathrm{sim}}_{\mathrm{Z}(\nu\nu)\mathrm{+jets}}} \tag{8.1}$$

are obtained from simulation, where $n^{\mathrm{sim}}_{\mathrm{V+jets}}$ and $n^{\mathrm{sim}}_{\mathrm{Z}(\nu\nu)\mathrm{+jets}}$ are the expected bin yields of a targeted V+jets process in a specific analysis region and of Z$(\nu\nu)$+jets in the SR, respectively. In total, six V+jets processes in the SR and CRs are expressed as the product of a TF and the freely floating estimate $r^{\mathrm{Z}(\nu\nu)}$, namely:

- W$(\ell\nu)$+jets in the SR;
- Z$(\ell\ell)$+jets in the Z(ee) and Z$(\mu\mu)$ CRs;
- W$(\ell\nu)$+jets in the W$(\mathrm{e}\nu)$ and W$(\mu\nu)$ CRs;
- W$(\ell\nu)$+jets in the t$\bar{\mathrm{t}}(\mathrm{e}\nu)$ and t$\bar{\mathrm{t}}(\mu\nu)$ CRs;
- $\gamma$+jets in the $\gamma$ CR.

This causes $r^{\mathrm{Z}(\nu\nu)}$ to be strongly constrained in the fit using data from the V+jets CRs.

JHEP09(2025)141

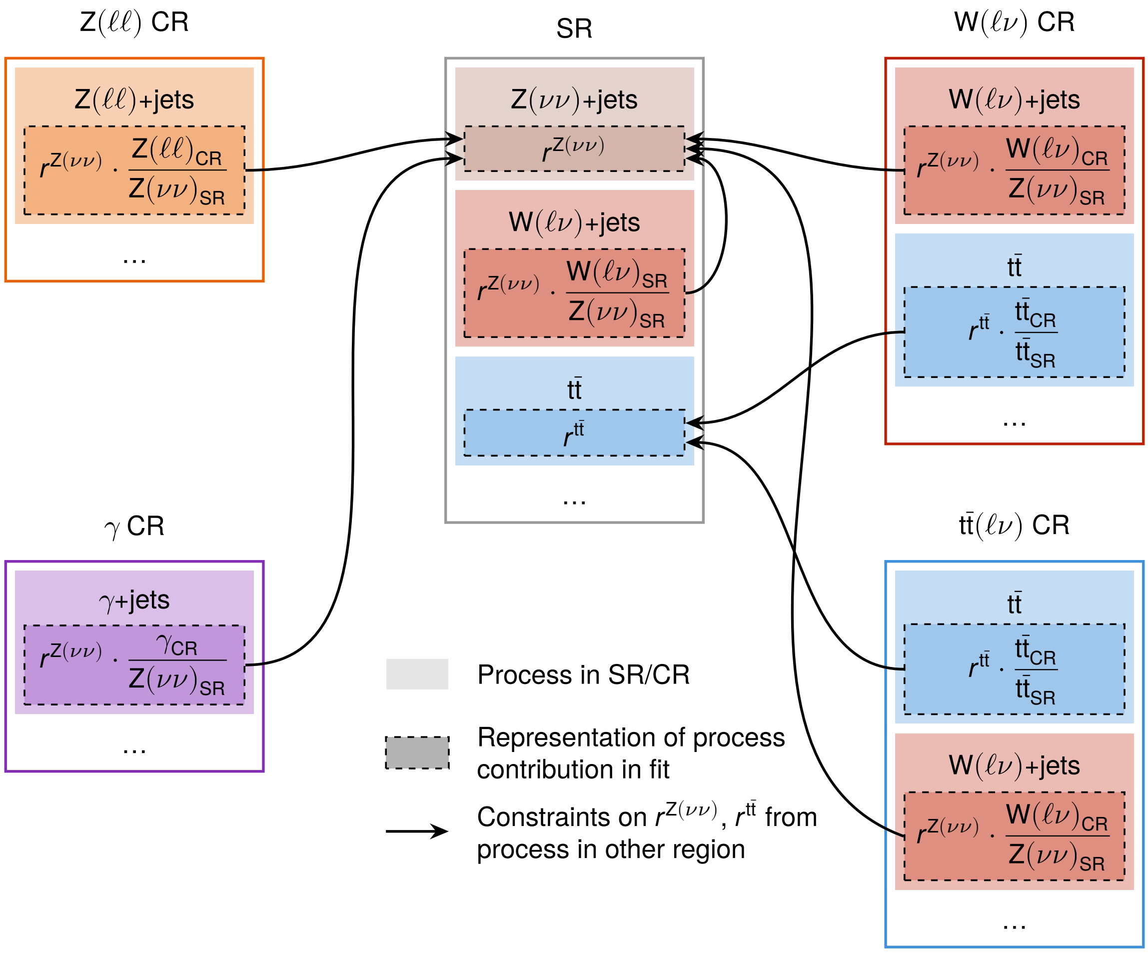


**Figure 5.** Statistical model used for the estimation of the major background processes for one bin of the $R_T$ distribution. The contributions of $Z(\nu\nu)$+jets and $t\bar{t}$ production in the SR are estimated with freely floating parameters $r^{Z(\nu\nu)}$ and $r^{t\bar{t}}$. Constraints on $Z(\nu\nu)$+jets production are obtained by expressing similar processes in the SR and CRs as products of $r^{Z(\nu\nu)}$ and a TF, obtained from simulation. Concerning $t\bar{t}$ production, the $t\bar{t}$ processes in the $t\bar{t}(\ell\nu)$ and $W(\ell\nu)$ CRs are expressed in terms of $r^{t\bar{t}}$ and a TF. All processes not depicted in this illustration are estimated using simulated events. Regions containing charged leptons are included twice in this model, once for electrons and once for muons. The model is implemented for the t-pass and t-fail regions separately.

Similarly, the $R_T$ distribution of $t\bar{t}$ production in the SR is estimated as freely floating parameter $r^{t\bar{t}}$ for each bin of the distribution. Here, the contribution of $t\bar{t}$ production to CRs is used to constrain $r^{t\bar{t}}$:

- $t\bar{t}$ in the $t\bar{t}(e\nu)$ and $t\bar{t}(\mu\nu)$ CRs;
- $t\bar{t}$ in the $W(e\nu)$ and $W(\mu\nu)$ CRs.

In both cases, the TF model is implemented independently for the t-pass and the t-fail regions. Figure 5 shows the full TF model, as implemented in this search, for one bin of the $R_T$ distribution.

The simulated yields in the TFs, as defined in eq. (8.1), are subject to systematic uncertainties. Their effects are propagated to the TFs by varying the corresponding simulated yields in the corresponding nuisance parameters. All systematic uncertainties, listed in section 9, are propagated to the TFs. Since the TFs are ratios of similar processes in different CRs, several systematic uncertainties affect the numerator and denominator in the TF in a comparable way. Because of this, these uncertainties are significantly reduced in the TFs.

To evaluate the importance of the CRs and TFs employed in the statistical model, fits in different scenarios with some CRs left out have been performed with the signal $m_{\mathrm{M}} = 2000\,\mathrm{GeV}$, $m_\chi = 150\,\mathrm{GeV}$ on Asimov pseudodata. The results on the expected uncertainties in $r^{\mathrm{Z}(\nu\nu)}$ in these fits are compared to a fit on a statistical model including all CRs. In these fits, the $r^{\mathrm{t\bar{t}}}$ parameters have been fixed to the nominal yield of $\mathrm{t\bar{t}}$ in the corresponding bin from simulation in order to isolate the effect on the $\mathrm{Z}(\nu\nu)$+jets estimation. When excluding the $\mathrm{Z}(\ell\ell)$ CRs, effectively removing TFs with the $\mathrm{Z}(\ell\ell)$+jets process from the fit model, the uncertainty on $r^{\mathrm{Z}(\nu\nu)}$ increases by 50% in low-$R_{\mathrm{T}}$ and by 10% in high-$R_{\mathrm{T}}$ bins. When excluding the $\mathrm{W}(\ell\nu)$ and the $\mathrm{t\bar{t}}$ CRs, effectively removing TFs with the $\mathrm{W}(\ell\nu)$+jets process in CRs, the uncertainty on $r^{\mathrm{Z}(\nu\nu)}$ increases by 90% in low-$R_{\mathrm{T}}$ and by 30% in high-$R_{\mathrm{T}}$ bins. The relative uncertainty of $r^{\mathrm{Z}(\nu\nu)}$ is approximately constant across the $R_{\mathrm{T}}$ range in these two scenarios. When the $\gamma$ CRs are left out of the fit, which removes the $\gamma$ TFs from the fit, the uncertainty increases by around 20% in low-$R_{\mathrm{T}}$ and by around 60% in high-$R_{\mathrm{T}}$ bins. The relative uncertainty in $r^{\mathrm{Z}(\nu\nu)}$ increases for larger $R_{\mathrm{T}}$. Hence, concerning the TF method, the $\gamma$ CRs can put additional constraints on $r^{\mathrm{Z}(\nu\nu)}$ in the high-$R_{\mathrm{T}}$ region compared to the other processes involved in the TF method.

Bias studies have confirmed that no bias on the fitted signal cross section is induced using this statistical model.

The modeling of QCD multijet production is validated in the SR by comparing the $R_{\mathrm{T}}$ distribution obtained from simulation with a shape extracted from a data-driven approach. For each SR, a dedicated, mutually exclusive determination region (DR) enriched in QCD multi-jet events is built by applying all selection criteria for the SR except for the requirements on $\Delta\phi(\mathrm{AK4~jets}, \vec{R}_{\mathrm{T}})$ and $\Delta\phi(\mathrm{AK15~jet}, \vec{R}_{\mathrm{T}})$. Events in the DRs must have at least one AK4 jet with $\Delta\phi(\mathrm{AK4~jet}, \vec{R}_{\mathrm{T}}) < 0.5$, and the requirement of $\Delta\phi(\mathrm{AK15~jet}, \vec{R}_{\mathrm{T}}) > 1.5$ is lifted. The $R_{\mathrm{T}}$ distribution of QCD multijet production in the DR is estimated by subtracting the background yield of remaining processes, obtained from simulation, from the data yield in each bin of the $R_{\mathrm{T}}$ distribution. The derived $R_{\mathrm{T}}$ distribution of QCD multijet production in the DR is mapped to the SR by multiplying the bin yield in the DR by dedicated TFs derived from a simulation of QCD multijet production. The TFs are computed in each bin of the $R_{\mathrm{T}}$ distribution by dividing the predicted QCD multijet yield in the SR by the predicted QCD multijet yield in the corresponding DR.

The closure of the QCD multijet simulation is tested in the SRs by comparing the predicted $R_{\mathrm{T}}$ distributions, derived from simulation, and from an estimate based on control samples in data. The difference between the predicted distributions from simulation and data ranges from 10 to 75%, depending on $R_{\mathrm{T}}$. The simulation consistently underestimates the predicted number of QCD multijet events in the SR, compared to the distribution obtained from data. The contamination of the SR with events from QCD multijet production is less than 1%, compared to the total expected SM background, hence the contribution of QCD multijet production is expected to have a negligible impact on the total predicted SM background in the SRs. In conclusion, simulated events are used to estimate the contribution of QCD multijet production. To express the difference between the distributions obtained from simulation and from control samples in data, a normalization uncertainty of 100% is assumed on the predicted yield of QCD multijet production in simulation.

## 9 Systematic uncertainties

Several sources of experimental and theoretical uncertainty are considered in this analysis. All systematic uncertainties are implemented as constrained nuisance parameters in the statistical model and are propagated to the final distributions and TFs after the simultaneous binned maximum likelihood fit used for signal extraction. The systematic uncertainties can be grouped into two types: normalization and/or shape. Normalization uncertainties only affect the total expected event yield. Shape uncertainties can affect both the total number of events and the distribution of the final measured hadronic recoil. Only systematic uncertainties that are directly related to the processes in figure 5 have an influence on the TFs.

In the following, the sources of systematic uncertainty considered in this analysis are described. Unless otherwise stated, the systematic uncertainties are implemented as shape uncertainties.

- *Renormalization and factorization scales*: for the major backgrounds ($\mathrm{t\bar{t}}$, W+jets, Z+jets, $\gamma$+jets, and single t production) and the signal process the matrix element renormalization and factorization scales were varied up and down independently by a factor of 2 and 0.5, respectively. The uncertainties in the renormalization and factorization scale account for missing higher-order processes in the simulation. The up and down shifts are propagated to the simultaneous fit. The renormalization and factorization scale uncertainty for each process is uncorrelated during the fitting process. A 100% correlation of these uncertainties across all data-taking periods is assumed.

- *Parton distribution functions*: for the simulated samples, the PDFs are taken from NNPDF (v. 3.1) [58] and are used to evaluate the uncertainty associated with the choice of PDF. The 100 variations of the PDF set are determined using the eigenvector or Hessian [86, 87] approach and are then used to construct a 68% confidence interval envelope around the nominal PDF value. This envelope is used as a shape uncertainty. The PDF uncertainties are assumed to be 100% correlated for major background processes, which are mostly initiated by the same partons (namely a qg or a gg initial state). Processes with different initial states are treated as uncorrelated. The PDF uncertainty on the signal process is assumed to be uncorrelated with those on all background processes. In addition, the uncertainty in $\alpha_S$ is propagated to the PDFs, which is treated as an additional shape uncertainty. This uncertainty is treated as 100% correlated across all background processes. All of the presented uncertainties are 100% correlated across all data-taking periods.

- *Initial- and final-state radiation (ISR and FSR)*: the parton shower scale in the simulation of major background samples was varied up and down by factors of 2 and 0.5, respectively, to evaluate the impact of $\alpha_S$ on parton showers. The weights are obtained directly from simulation and used to generate input templates to the simultaneous fit. The

ISR and FSR uncertainties are varied independently during the fitting procedure. These uncertainties are assumed to be 100% correlated between the different data-taking periods for all the major backgrounds and uncorrelated between the signal prediction and background processes. ISR and FSR uncertainties are correlated across all data-taking periods.

- *Top quark $p_{\mathrm{T}}$ reweighting*: the top quark $p_{\mathrm{T}}$ distribution of simulated $\mathrm{t\bar{t}}$ events is reweighted to NNLO(QCD)+NLO(EW) predictions [88]. The simulation without reweighting and the doubled effect of the reweighting procedure are used as uncertainty of this method. This uncertainty is 100% correlated across all data-taking periods.

- *SM cross sections*: for the minor background processes of diboson and QCD multijet production, the uncertainties in the renormalization scale, the factorization scale, and the PDFs are replaced by an overall normalization uncertainty in the cross section predictions of these processes. The rate uncertainty in the total cross section of diboson production [78–80] is 5%. An uncertainty of 100% is assigned to the total cross section of QCD multijet production, as described in section 8. The cross section uncertainty is correlated across all taking periods for each process.

- V+jets *electroweak correction*: the W+jets, Z+jets, and $\gamma$+jets background models are reweighted to account for NLO EW corrections, as described in ref. [77]. The theoretical uncertainties as functions of the vector boson $p_{\mathrm{T}}$ are provided by the authors and are applied to the W+jets, Z+jets, and $\gamma$+jets samples. Altogether there are three sources of EW uncertainties: the unknown Sudakov logarithms beyond NNLO and/or next-to-leading logarithmic accuracy, the unknown hard (non-Sudakov) EW corrections beyond NLO, and the process-correlation effects. For the other two sources, the correlation across the processes is unknown, therefore no correlation is assumed for them. The uncertainties are correlated across all data-taking periods.

- *Integrated luminosity*: the uncertainty in the measurement of the integrated luminosity is broken up into five separate parts [89–91]. There are three uncorrelated parts that are specific to the year in which the data were collected and two correlated parts. The first affects all three data-taking years, while the second only affects the last two data-taking years. They are implemented as normalization uncertainties of both the background and signal rates, with a range between 0.2 and 2.0%.

- *Lepton reconstruction and identification*: the reconstruction and identification efficiency for electrons, and the identification and isolation efficiency for muons in simulation is corrected to the performance observed in data from $\mathrm{Z}/\gamma^* \to \ell\ell$ events, as a function of the lepton $p_{\mathrm{T}}$ and $\eta$. Each of the four corrections is derived independently. Due to the small size of the uncertainties, the statistical and systematic components of the uncertainty are combined and propagated to the simultaneous fit. The muon and electron uncertainties are uncorrelated from one another. Each of the four aforementioned uncertainties is correlated across CRs in the same data-taking period. As the efficiencies and associated uncertainties are dependent on detector configuration, they are uncorrelated across different data-taking periods.



JHEP09(2025)141

- *Photon identification*: the identification efficiency for photons in simulation is corrected to the performance observed in data as a function of the photon's $p_{\mathrm{T}}$ and $\eta$. Due to the small size of the uncertainty the statistical and systematic components are combined and propagated to the final simultaneous fit. The uncertainty is uncorrelated across data-taking periods.

- *Trigger efficiency*: the efficiency for electron, photon, and $p_{\mathrm{T}}^{\text{miss, no }\mu}$ triggers is measured in data and residual differences to the efficiency in simulation are corrected [37]. The uncertainty associated with this correction is binned in $p_{\mathrm{T}}$ and $\eta$ for the lepton and photon trigger and in $p_{\mathrm{T}}^{\text{miss}}/R_{\mathrm{T}}$ for the $p_{\mathrm{T}}^{\text{miss, no }\mu}$ trigger and is propagated to the statistical model. The $p_{\mathrm{T}}^{\text{miss, no }\mu}$ and single photon trigger efficiency is measured in an orthogonal sideband region and the single electron trigger efficiency is calculated using a tag-and-probe approach. The trigger efficiency uncertainty is correlated across CRs and SRs that utilize the same trigger. The uncertainty is uncorrelated across data-taking periods.

- *Level-1 prefiring*: during operation, a gradual timing shift of the ECAL was not properly propagated to the L1 trigger primitives (TP), resulting in a significant fraction of high-$\eta$ TP being mistakenly associated to the previous bunch crossing. Since L1 trigger rules forbid two consecutive bunch crossings to fire, a consequence of this is that events can self veto if a significant amount of ECAL energy is found in the region of $2 < \eta < 3$ (L1 ECAL prefiring). The effect is not described genuinely by the simulation but taken into account using event weights. This effect is most prominent in the 2016 and 2017 data-taking periods. The effects of the mistiming of the L1 ECAL trigger is propagated to the statistical model. The uncertainty is uncorrelated across the data-taking periods and applies only to the 2016 and 2017 data-taking years.

- *Pileup*: the uncertainty in the distribution of the number of pileup interactions in the events is evaluated by varying the total inelastic pp cross section in the simulation by $\pm 4.6\%$ [92]. To accommodate different beam and detector conditions, the uncertainty is uncorrelated across all data-taking periods.

- *Jet energy scale*: the uncertainty associated with the jet energy scale correction is estimated by shifting the jet energy scale up and down one standard deviation according to the source of uncertainty and then re-analyzing all the data with shifted jet energies [46, 93, 94]. Altogether eleven different sources of uncertainty in the jet energy scale are considered. The jet energy scale uncertainty is uncorrelated or correlated across data-taking periods depending on the source of uncertainty. A dedicated additional uncertainty is considered for the 2018 data set to account for any remaining effect of the HEM issue.

- *Jet energy resolution*: the uncertainty in the jet energy resolution correction is evaluated by increasing or decreasing the difference between the reconstructed and particle-level jet energies [46, 93, 94]. The total uncertainty of this process is propagated to the final simultaneous fit and is uncorrelated across the data-taking periods.



JHEP09(2025)141

- $p_T^{miss}$ *unclustered energy*: the uncertainty in the $p_T^{miss}$ calculation from unclustered energy is estimated by varying each particle type by its estimated resolution. This uncertainty is uncorrelated across data-taking periods.

- *Jet* b *tagging*: the b tagging scale factors, and their associated uncertainties, are dependent on the properties of the jet [95]. The uncertainty in the selection efficiency and misidentification rate are propagated to the statistical model. There is one selection and one misidentification uncertainty that are correlated across all data-taking periods and eight selection and misidentification uncertainties that are not correlated across the data-taking periods.

- *Jet* t *tagging*: the selection efficiencies of the ParticleNet t tagger [33] in simulation are corrected with scale factors to match the corresponding data efficiencies. The uncertainties depend on the type of AK15 jet (t jet, QCD jet, or b jet) and on its kinematic properties. The uncertainty in the scale factor of the t tagging efficiency is 9–16%. The uncertainty in the scale factor of the misidentification rate of an AK15 QCD jet is 12–18%. As events with misidentified AK15 b jets only represent a minor contribution, a scale factor of 1 and an uncertainty of 50% on it is assumed. The misidentification rate uncertainties largely cancel in the TFs, which reduces the impact of these uncertainties in the fit presented in section 10. The uncertainties in the t tagging efficiency and misidentification rate are uncorrelated across data-taking periods.

- *Limited size of simulation samples*: the limited size of the samples of simulated events results in statistical fluctuations on the nominal prediction. This uncertainty is taken into account with the simplified Barlow-Beeston method [96]. For bins with more than ten unweighted entries, a single Gaussian constrained nuisance parameter is introduced to each bin that scales the total yield. A Poisson probability distribution function is used for bins with fewer than ten entries.

## 10 Results and interpretation

The postfit distributions of the hadronic recoil in the SRs for a fit to the background-only hypothesis are shown in figure 6. The data are found to be in agreement with the SM prediction within uncertainties. A goodness-of-fit test with the saturated model [97] was performed to quantify the level of agreement of the data and the background-only postfit model that yielded a $p$-value of 0.72. The postfit distributions in the CRs are shown in appendix A.

In addition, binned maximum likelihood fits of signal-plus-background hypotheses to data are performed. Each tested signal-plus-background hypothesis is characterized by the choice of the unknown mediator mass and the DM candidate mass. No significant deviation from the SM expectation is found in these fits. Exclusion limits on the production strength of the mono-top signal, namely the product of the cross section and the branching fraction ($\sigma\mathcal{B}$) of $\mathrm{pp} \to \mathrm{tM}(\chi\overline{\chi})$ production, are presented as functions of mediator masses between 200 and 2250 GeV and DM candidate masses between 1 and 1225 GeV, only considering on-shell decays of the mediator to the DM candidates. The exclusion limits at 95% confidence level (CL) are calculated using the asymptotic approximation of the $\mathrm{CL_s}$ criterion [98–100] using

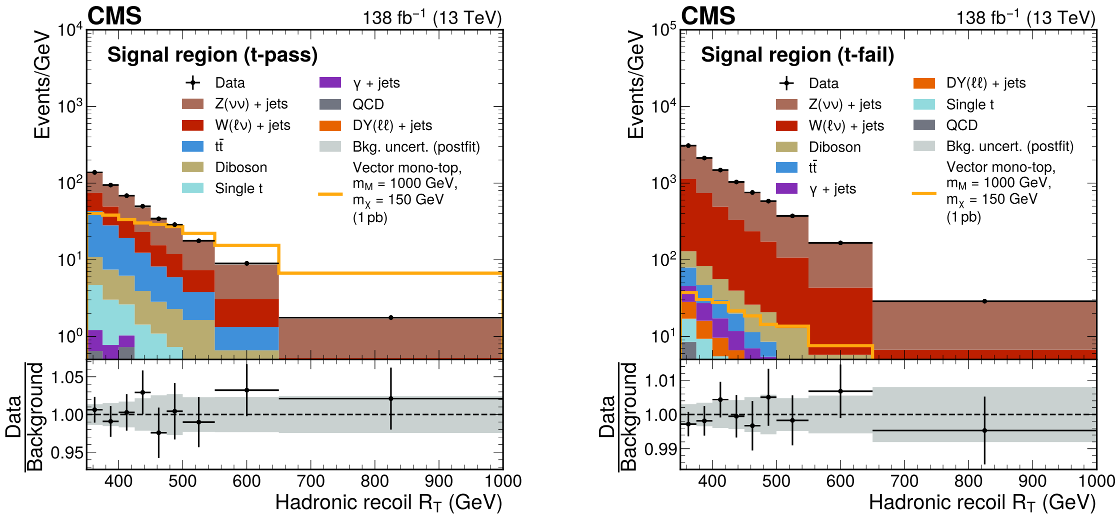


**Figure 6.** Postfit distributions of the magnitude of the hadronic recoil $R_{\mathrm{T}}$ in the SR (t-pass) and SR (t-fail) after a fit of the background model to the data. The last bin of each distribution also contains events with $R_{\mathrm{T}} > 1000\,\mathrm{GeV}$. The background processes are stacked together. A representative mono-top signal (vector coupling scenario) with a mediator mass of 1 TeV, a DM candidate mass of 150 GeV, and a cross section of 1 pb is overlaid as an orange line. The gray band represents the statistical and postfit systematic uncertainties in the predicted background yields after the fit.

the LHC test statistic. The observed and expected limits are calculated as function of $m_{\mathrm{M}}$ for a constant $m_\chi = 150\,\mathrm{GeV}$. For fixed values of $m_{\mathrm{M}}$, the limit on $\sigma\mathcal{B}$ is assumed to be constant as function of $m_\chi$. The signal shape of the hadronic recoil distribution does not depend on $m_\chi$ if the DM production is on-shell, making such an extrapolation valid.

The impact of systematic uncertainties is checked for a signal with a vector mediator and with $m_{\mathrm{M}} = 2000\,\mathrm{GeV}$ and $m_\chi = 150\,\mathrm{GeV}$. For this signal hypothesis, the expected exclusion limit roughly corresponds to the theory prediction of $\sigma\mathcal{B}$, promoting this hypothesis to a representative signal close to the expected exclusion contour. An uncertainty breakdown of the fit shows that statistical and systematic uncertainties on the best fit $\sigma\mathcal{B}$ are at a similar level. The expected exclusion limit is calculated with nuisance parameters related to a group of systematic uncertainties fixed. The relative change of the limit compared to the fit on the full statistical model is used to quantify the impact of the systematic uncertainty on the results of the search. The numerical results are summarized in table 3. The largest impacts on the expected exclusion limit come from the uncertainties in the renormalization and factorization scales of the background processes, and from the limited size of the simulated samples.

Figure 7 shows the expected upper exclusion limits at 95% CL on the production strength $\sigma\mathcal{B}$ of mono-top production as a function of the mediator and DM candidate mass assuming vector (upper part) and axial-vector (lower part) couplings exclusively. For the vector (axial-vector) coupling scenario, $(g_{\mathrm{v}}^{U})_{13} = 0.25$ and $g_{\mathrm{v}}^{\chi} = 1$ ($(g_{\mathrm{v}}^{U})_{13} = 0.25$ and $g_{\mathrm{a}}^{\chi} = 1$) and all axial-vector (vector) couplings are set to zero. For both, the vector and axial-vector coupling scenarios, an exclusion of mediator masses of up to 1.85 TeV is observed, where 2.0 TeV is expected. For a mediator with pure vector (axial-vector) couplings, DM candidate masses of



JHEP09(2025)141

| Uncertainty group | Change in exclusion limit on $\sigma\mathcal{B}$ |
|---|---|
| Renormalization and factorization scale | 9.7% |
| Limited size of simulated samples | 6.9% |
| Remaining theory uncertainties | 5.5% |
| Remaining experimental uncertainties | 2.8% |
| All systematic uncertainties | 23.4% |

**Table 3.** Impact of systematic uncertainties on the expected exclusion limit for the vector mono-top signal with $m_{\mathrm{M}} = 2000\,\mathrm{GeV}$ and $m_{\chi} = 150\,\mathrm{GeV}$, quantified by the relative change in the expected exclusion limit when fixing the nuisance parameters related to a group of systematic uncertainties in the fit. The last row shows the impact on the exclusion limit if all nuisance parameters related to systematic uncertainties are fixed in the fit.

JHEP09(2025)141

up to 750 (550) GeV are excluded, where 850 (650) GeV is expected. The results of this search are comparable to a similar search [28] performed by the ATLAS collaboration using an alternative coupling scenario with couplings $(g_{\mathrm{V}}^{U})_{13} = 0.5$ and $g_{\mathrm{V}}^{\chi} = 1$, and a direct comparison can be made using the results in appendix B.

The exclusion of mediator and DM candidate masses coming from DM relic constraints measured by the Planck collaboration [3] is shown as a solid gray line. For this line the measured value of the density of DM or nonbaryonic matter $\Omega_{\mathrm{nbm}}h^2 = 0.12$ is used with $h$ representing the reduced Hubble constant. Here, $\Omega_{\mathrm{nbm}}h^2$ is the faction of the observable universe that is composed of nonrelativistic dark matter. Mediator and DM candidate masses in the areas indicated by the hatched side of the solid gray contour in figure 7 result in higher relic densities than observed and are therefore excluded. The relic densities for the corresponding mono-top models were calculated using MadDM [101, 102].

## 11 Summary

A search for dark matter (DM) produced in association with a single top quark via a flavor changing neutral current, referred to as nonresonant mono-top production, was presented. The analysis was performed using data collected by the CMS experiment in 2016, 2017, and 2018 at the LHC at a center-of-mass-energy of 13 TeV, and corresponding to an integrated luminosity of $138\,\mathrm{fb}^{-1}$.

The Lorentz boost of the top quark is exploited to cluster the products of the hadronic top quark decay into a large-radius jet. Furthermore, a machine-learning-based discriminator is used to distinguish large-radius jets originating from hadronic top quark decays and large-radius jets produced purely through quantum chromodynamics processes. A robust statistical model was built to determine the main backgrounds in the signal regions using data in dedicated control regions. The distribution of the hadronic recoil in the signal and control regions is used to perform the statistical fit to the data.

The data are consistent with the background-only hypothesis, and no evidence for DM produced in association with a single top quark was found. Limits at 95% confidence level are calculated for the product of the signal production cross section and the branching fraction of the mediator decaying into DM candidates. Limits were obtained for both a

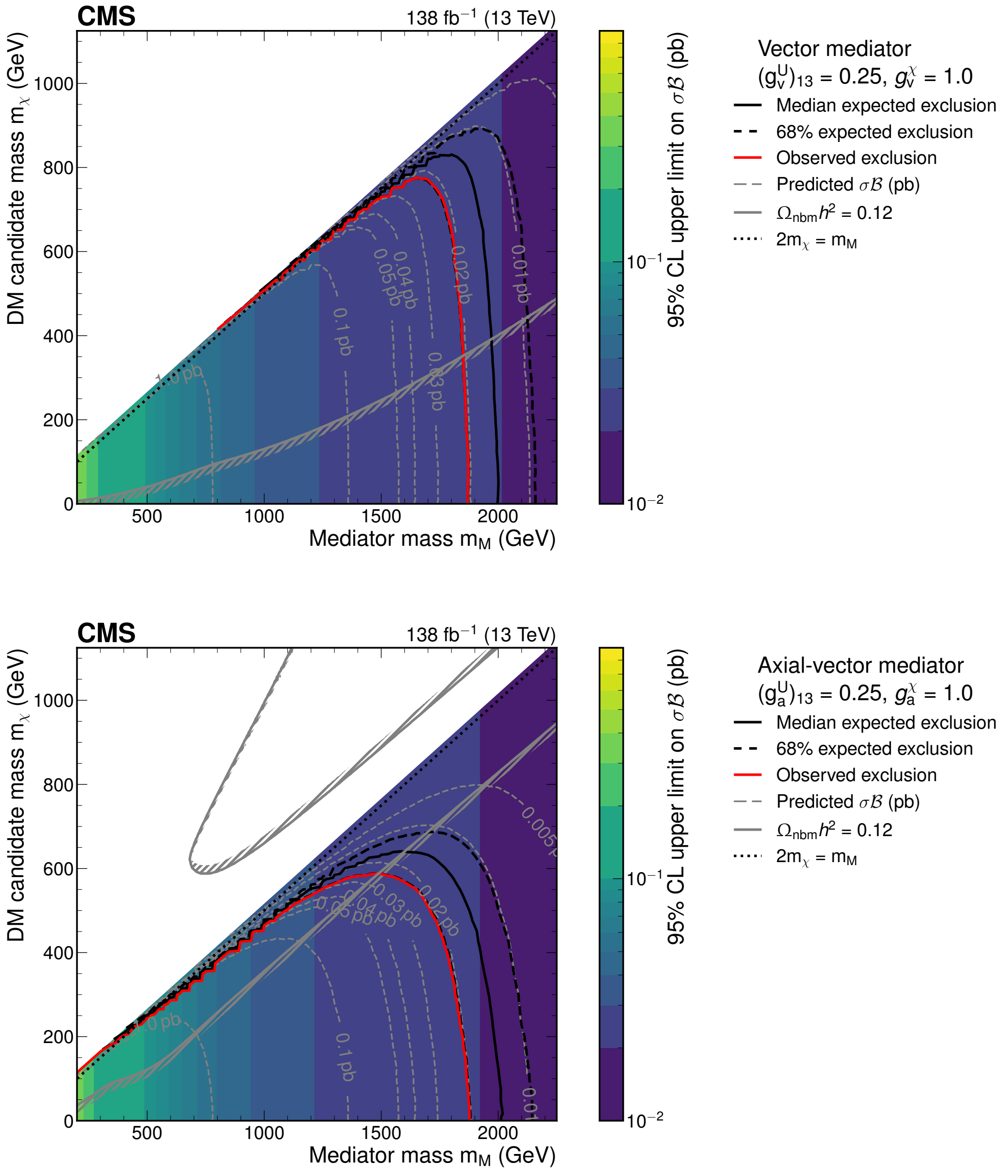


**Figure 7.** Upper limits at 95% CL on $\sigma\mathcal{B}$ of mono-top production presented in the two-dimensional plane spanned by the mediator and DM candidate masses for a mediator mass between 200 and 2250 GeV and a DM candidate mass between 1 and 1125 GeV only considering on-shell decays of the mediator to the DM candidates. The mediator has vector couplings to quarks and DM candidates in the upper plot and axial-vector couplings in the lower plot. The median expected exclusion range is indicated by a black solid line, demonstrating the search sensitivity of the analysis. The 68% probability interval of the expected exclusion is shown in black dashed lines. Contours of theory predictions for constant values of $\sigma\mathcal{B}$ are shown in gray dashed lines. The observed exclusion contour of mediator and DM candidate masses is represented by the red solid line. The exclusion contour obtained from measurements of the DM relic density $\Omega_{\text{nbm}}h^2$ by the Planck collaboration is shown in the gray solid line.

JHEP09(2025)141

purely vector and a purely axial-vector mediator that couples to two DM candidates and to two standard model quarks: one from the first generation and another from the third. The analysis excludes mediators with masses up to 1.85 TeV, where 2.0 TeV is expected, for both the vector and the axial-vector coupling scenarios. Dark matter candidate masses below 750 (550) GeV, where 850 (650) GeV is expected, are excluded for the vector (axial-vector) coupling scenario. In both cases, the exclusion limits are calculated for mediator masses greater than 200 GeV and DM candidate masses greater than 1 GeV. The exclusion limit on the spin-1 mediator mass obtained in this search exceeds the previous CMS result on mono-top production [27] using the 2016 data set by 100 GeV.


## Acknowledgments

We congratulate our colleagues in the CERN accelerator departments for the excellent performance of the LHC and thank the technical and administrative staffs at CERN and at other CMS institutes for their contributions to the success of the CMS effort. In addition, we gratefully acknowledge the computing centers and personnel of the Worldwide LHC Computing Grid and other centers for delivering so effectively the computing infrastructure essential to our analyses. Finally, we acknowledge the enduring support for the construction and operation of the LHC, the CMS detector, and the supporting computing infrastructure provided by the following funding agencies: SC (Armenia), BMBWF and FWF (Austria); FNRS and FWO (Belgium); CNPq, CAPES, FAPERJ, FAPERGS, and FAPESP (Brazil); MES and BNSF (Bulgaria); CERN; CAS, MoST, and NSFC (China); MINCIENCIAS (Colombia); MSES and CSF (Croatia); RIF (Cyprus); SENESCYT (Ecuador); ERC PRG, RVTT3 and MoER TK202 (Estonia); Academy of Finland, MEC, and HIP (Finland); CEA and CNRS/IN2P3 (France); SRNSF (Georgia); BMBF, DFG, and HGF (Germany); GSRI (Greece); NKFIH (Hungary); DAE and DST (India); IPM (Iran); SFI (Ireland); INFN (Italy); MSIP and NRF (Republic of Korea); MES (Latvia); LMTLT (Lithuania); MOE and UM (Malaysia); BUAP, CINVESTAV, CONACYT, LNS, SEP, and UASLP-FAI (Mexico); MOS (Montenegro); MBIE (New Zealand); PAEC (Pakistan); MES and NSC (Poland); FCT (Portugal); MESTD (Serbia); MICIU/AEI and PCTI (Spain); MOSTR (Sri Lanka); Swiss Funding Agencies (Switzerland); MST (Taipei); MHESI and NSTDA (Thailand); TUBITAK and TENMAK (Turkey); NASU (Ukraine); STFC (United Kingdom); DOE and NSF (U.S.A.).

Individuals have received support from the Marie-Curie program and the European Research Council and Horizon 2020 Grant, contract Nos. 675440, 724704, 752730, 758316, 765710, 824093, 101115353, 101002207, and COST Action CA16108 (European Union); the Leventis Foundation; the Alfred P. Sloan Foundation; the Alexander von Humboldt Foundation; the Science Committee, project no. 22rl-037 (Armenia); the Fonds pour la Formation à la Recherche dans l'Industrie et dans l'Agriculture (FRIA-Belgium); the Beijing Municipal Science & Technology Commission, No. Z191100007219010 and Fundamental Research Funds for the Central Universities (China); the Ministry of Education, Youth and Sports (MEYS) of the Czech Republic; the Shota Rustaveli National Science Foundation, grant FR-22-985 (Georgia); the Deutsche Forschungsgemeinschaft (DFG), among others, under Germany's Excellence Strategy – EXC 2121 "Quantum Universe" – 390833306, and under project number 400140256 - GRK2497; the Hellenic Foundation for Research and Innovation




JHEP09(2025)141

(HFRI), Project Number 2288 (Greece); the Hungarian Academy of Sciences, the New National Excellence Program - ÚNKP, the NKFIH research grants K 131991, K 133046, K 138136, K 143460, K 143477, K 146913, K 146914, K 147048, 2020-2.2.1-ED-2021-00181, TKP2021-NKTA-64, and 2021-4.1.2-NEMZ_KI-2024-00036 (Hungary); the Council of Science and Industrial Research, India; ICSC – National Research Center for High Performance Computing, Big Data and Quantum Computing and FAIR – Future Artificial Intelligence Research, funded by the NextGenerationEU program (Italy); the Latvian Council of Science; the Ministry of Education and Science, project no. 2022/WK/14, and the National Science Center, contracts Opus 2021/41/B/ST2/01369 and 2021/43/B/ST2/01552 (Poland); the Fundação para a Ciência e a Tecnologia, grant CEECIND/01334/2018 (Portugal); the National Priorities Research Program by Qatar National Research Fund; MICIU/AEI/10.13039/501100011033, ERDF/EU, "European Union NextGenerationEU/PRTR", and Programa Severo Ochoa del Principado de Asturias (Spain); the Chulalongkorn Academic into Its 2nd Century Project Advancement Project, and the National Science, Research and Innovation Fund via the Program Management Unit for Human Resources & Institutional Development, Research and Innovation, grant B39G670016 (Thailand); the Kavli Foundation; the Nvidia Corporation; the SuperMicro Corporation; the Welch Foundation, contract C-1845; and the Weston Havens Foundation (U.S.A.).

## A Postfit distributions in control regions

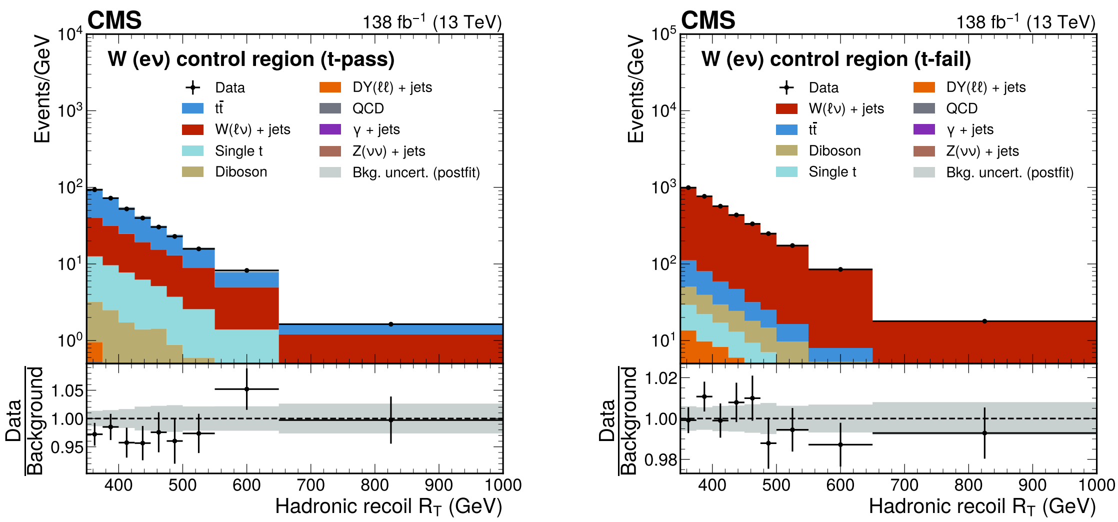


**Figure 8.** Postfit distributions of the magnitude of the hadronic recoil $R_{\mathrm{T}}$ in the W$(e\nu)$ (t-pass) and W$(e\nu)$ (t-fail) CRs after a fit of the background model to the data. The last bin of each distribution also contains events with $R_{\mathrm{T}} > 1000\,\mathrm{GeV}$. The background processes are stacked together. The gray band represents the statistical and postfit systematic uncertainties in the predicted background yields after the fit.



JHEP09(2025)141

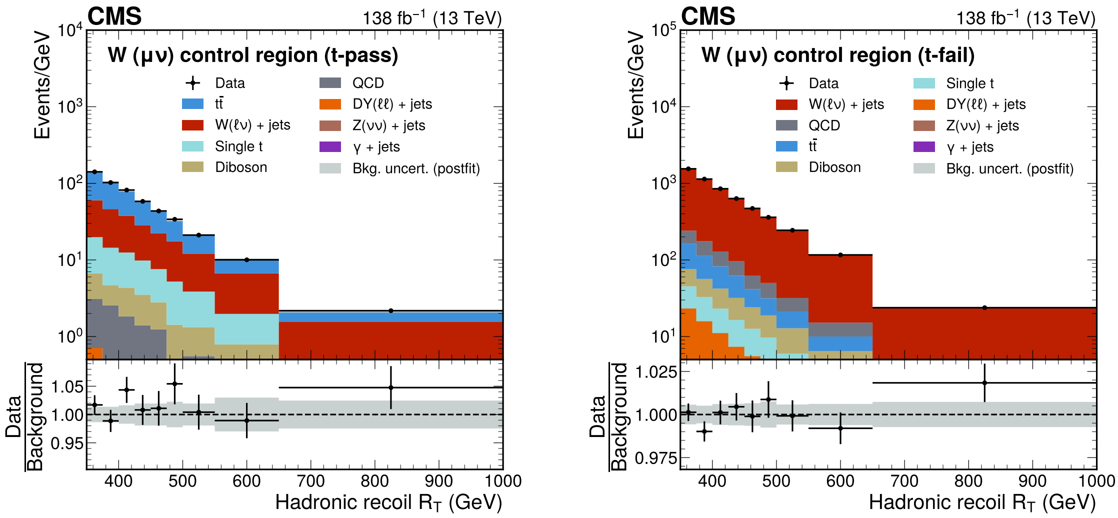


**Figure 9.** Postfit distributions of the magnitude of the hadronic recoil $R_{\mathrm{T}}$ in the $\mathrm{W}(\mu\nu)$ (t-pass) and $\mathrm{W}(\mu\nu)$ (t-fail) CRs after a fit of the background model to the data. The last bin of each distribution also contains events with $R_{\mathrm{T}} > 1000\,\mathrm{GeV}$. The background processes are stacked together. The gray band represents the statistical and postfit systematic uncertainties in the predicted background yields after the fit.

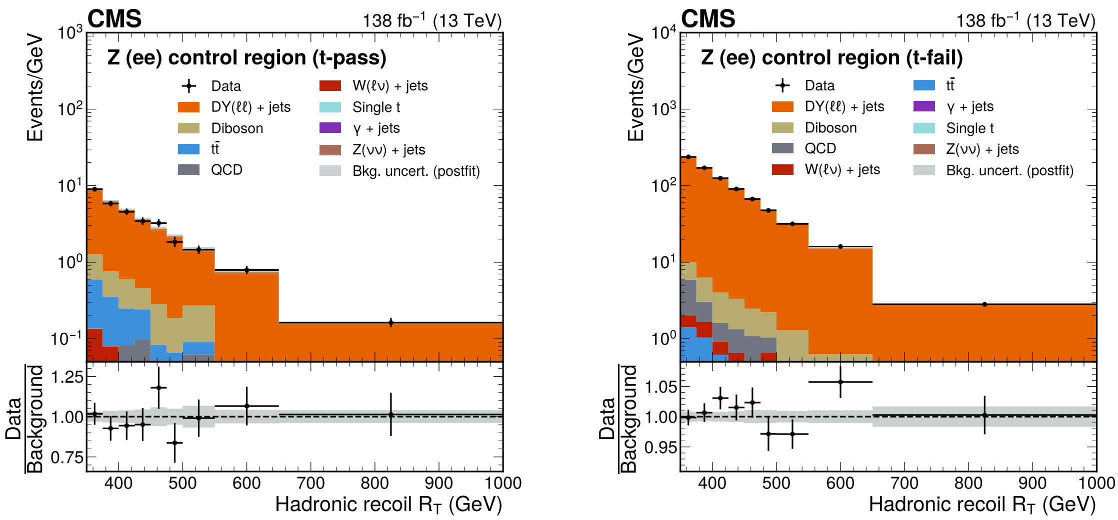


**Figure 10.** Postfit distributions of the magnitude of the hadronic recoil $R_{\mathrm{T}}$ in the Z(ee) (t-pass) and Z(ee) (t-fail) CRs after a fit of the background model to the data. The last bin of each distribution also contains events with $R_{\mathrm{T}} > 1000\,\mathrm{GeV}$. The background processes are stacked together. The gray band represents the statistical and postfit systematic uncertainties in the predicted background yields after the fit.



JHEP09(2025)141

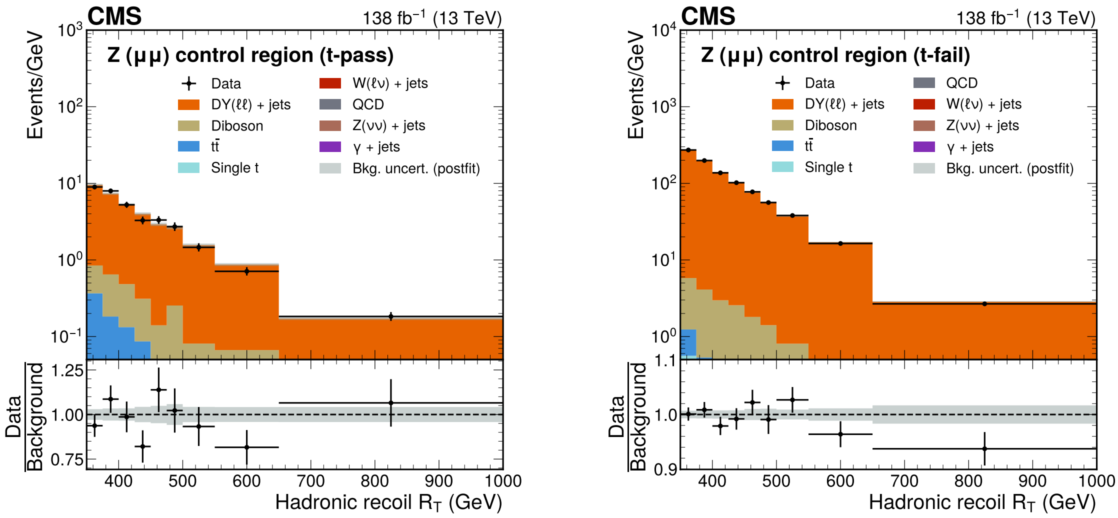


**Figure 11.** Postfit distributions of the magnitude of the hadronic recoil $R_\mathrm{T}$ in the $\mathrm{Z}(\mu\mu)$ (t-pass) and $\mathrm{Z}(\mu\mu)$ (t-fail) CRs after a fit of the background model to the data. The last bin of each distribution also contains events with $R_\mathrm{T} > 1000\,\mathrm{GeV}$. The background processes are stacked together. The gray band represents the statistical and postfit systematic uncertainties in the predicted background yields after the fit.

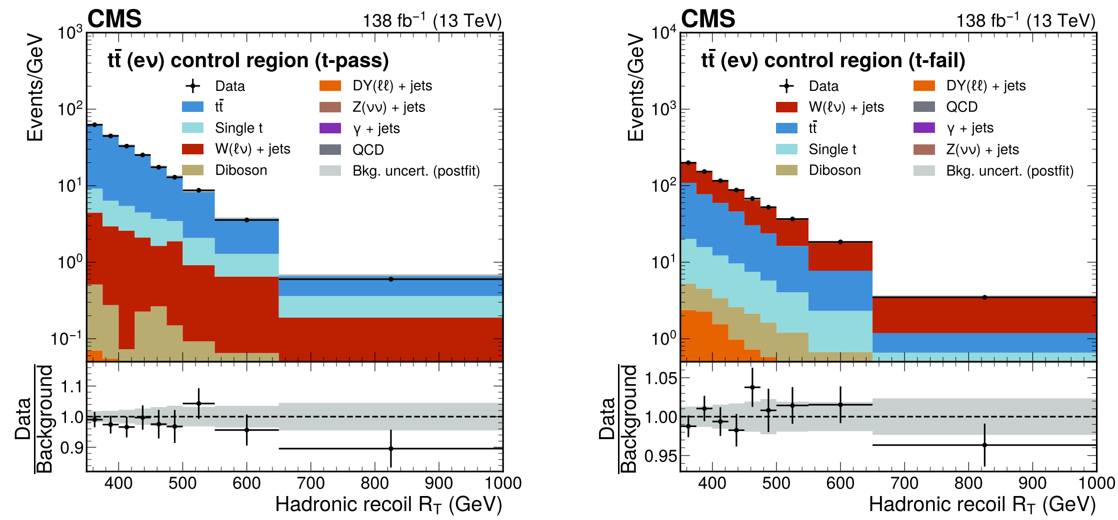


**Figure 12.** Postfit distributions of the magnitude of the hadronic recoil $R_\mathrm{T}$ in the $\mathrm{t\bar{t}}(\mathrm{e}\nu)$ (t-pass) and $\mathrm{t\bar{t}}(\mathrm{e}\nu)$ (t-fail) CRs after a fit of the background model to the data. The last bin of each distribution also contains events with $R_\mathrm{T} > 1000\,\mathrm{GeV}$. The background processes are stacked together. The gray band represents the statistical and postfit systematic uncertainties in the predicted background yields after the fit.

JHEP09(2025)141

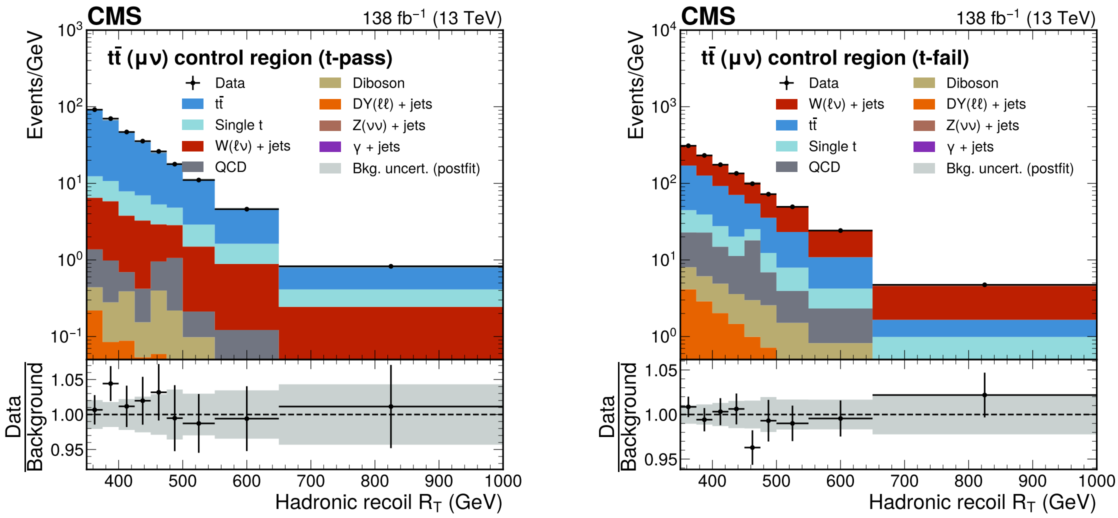


**Figure 13.** Postfit distributions of the magnitude of the hadronic recoil $R_T$ in the $t\bar{t}(\mu\nu)$ (t-pass) and $t\bar{t}(\mu\nu)$ (t-fail) CRs after a fit of the background model to the data. The last bin of each distribution also contains events with $R_T > 1000\,\mathrm{GeV}$. The background processes are stacked together. The gray band represents the statistical and postfit systematic uncertainties in the predicted background yields after the fit.

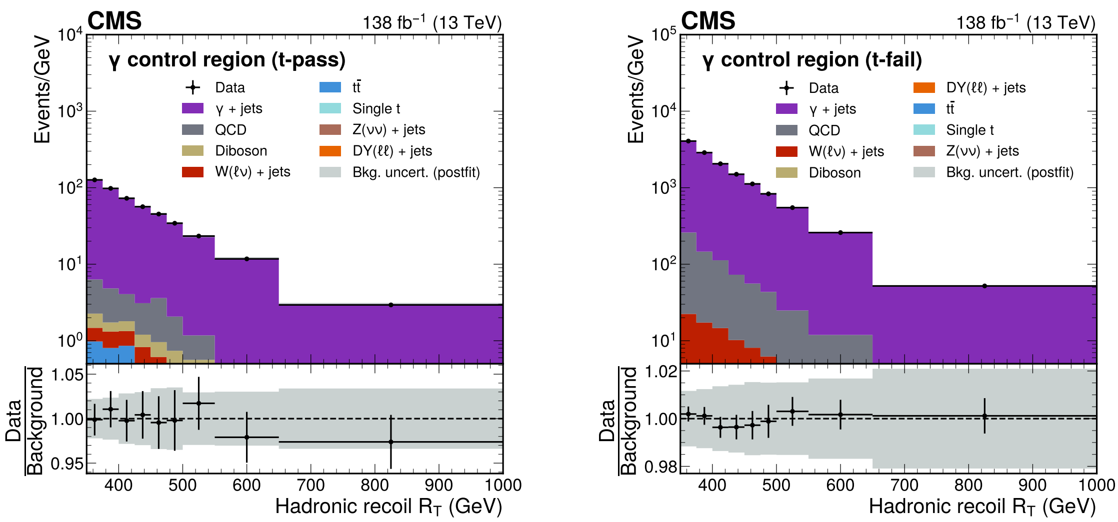


**Figure 14.** Postfit distributions of the magnitude of the hadronic recoil $R_T$ in the $\gamma$ (t-pass) and $\gamma$ (t-fail) CRs after a fit of the background model to the data. The last bin of each distribution also contains events with $R_T > 1000\,\mathrm{GeV}$. The background processes are stacked together. The gray band represents the statistical and postfit systematic uncertainties in the predicted background yields after the fit.

JHEP09(2025)141

## B Exclusion limits for alternative choice of couplings

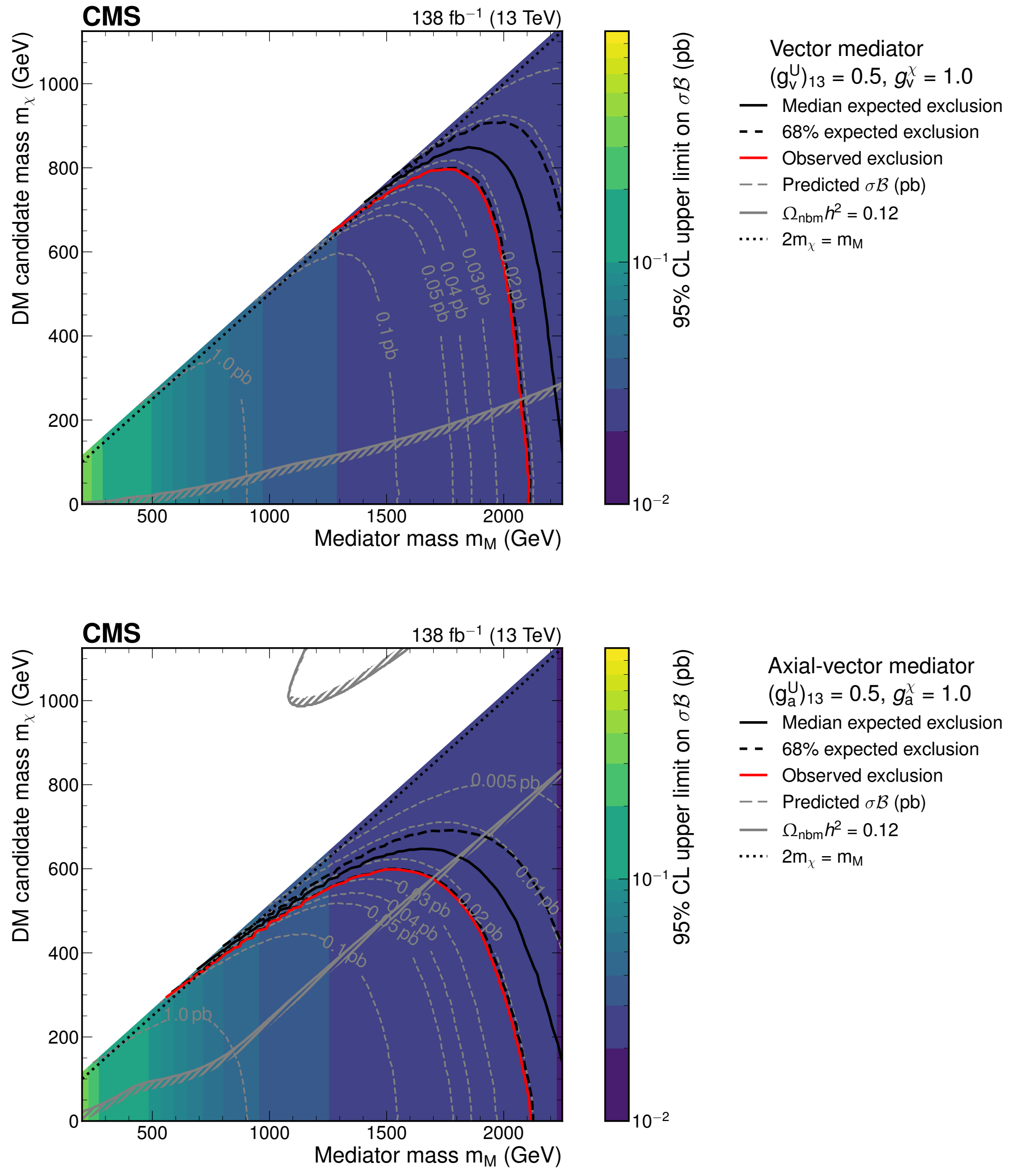


**Figure 15.** Upper limits at 95% CL on $\sigma\mathcal{B}$ of mono-top production presented in the two-dimensional plane spanned by the mediator and DM candidate masses for a mediator mass between 200 and 2250 GeV and a DM candidate mass between 1 and 1125 GeV only considering on-shell decays of the mediator to the DM candidates. The mediator has vector couplings to quarks and DM candidates in the upper plot and axial-vector couplings in the lower plot. The median expected exclusion range is indicated by a black solid line, demonstrating the search sensitivity of the analysis. The 68% probability interval of the expected exclusion is shown in black dashed lines. Contours of theory predictions for constant values of $\sigma\mathcal{B}$ are shown in gray dashed lines. The observed exclusion contour of mediator and DM candidate masses is represented by the red solid line. The exclusion contour obtained from measurements of the DM relic density $\Omega_{\mathrm{nbm}}h^2$ by the Planck collaboration is shown in the gray solid line.

JHEP09(2025)141

**Data Availability Statement.** This article has no associated data or the data will not be deposited. Release and preservation of data used by the CMS Collaboration as the basis for publications is guided by the CMS data preservation, re-use and open access policy.

**Code Availability Statement.** This article has no associated code or the code will not be deposited. The CMS core software is publicly available on GitHub.



## References


[1] V.C. Rubin and W.K. Ford Jr., *Rotation of the Andromeda Nebula from a Spectroscopic Survey of Emission Regions*, *Astrophys. J.* **159** (1970) 379 [INSPIRE].

[2] M. Markevitch et al., *Direct constraints on the dark matter self-interaction cross-section from the merging galaxy cluster 1E0657-56*, *Astrophys. J.* **606** (2004) 819 [astro-ph/0309303] [INSPIRE].

[3] Planck collaboration, *Planck 2018 results. VI. Cosmological parameters*, *Astron. Astrophys.* **641** (2020) A6 [*Erratum ibid.* **652** (2021) C4] [arXiv:1807.06209] [INSPIRE].

[4] M. Beltran, D. Hooper, E.W. Kolb, Z.A.C. Krusberg and T.M.P. Tait, *Maverick dark matter at colliders*, *JHEP* **09** (2010) 037 [arXiv:1002.4137] [INSPIRE].

[5] P.J. Fox, R. Harnik, J. Kopp and Y. Tsai, *Missing Energy Signatures of Dark Matter at the LHC*, *Phys. Rev. D* **85** (2012) 056011 [arXiv:1109.4398] [INSPIRE].

[6] J. Goodman, M. Ibe, A. Rajaraman, W. Shepherd, T.M.P. Tait and H.-B. Yu, *Constraints on Dark Matter from Colliders*, *Phys. Rev. D* **82** (2010) 116010 [arXiv:1008.1783] [INSPIRE].

[7] A. Rajaraman, W. Shepherd, T.M.P. Tait and A.M. Wijangco, *LHC Bounds on Interactions of Dark Matter*, *Phys. Rev. D* **84** (2011) 095013 [arXiv:1108.1196] [INSPIRE].

[8] ATLAS collaboration, *Search for new phenomena in final states with an energetic jet and large missing transverse momentum in pp collisions at $\sqrt{s} = 8$ TeV with the ATLAS detector*, *Eur. Phys. J. C* **75** (2015) 299 [*Erratum ibid.* **75** (2015) 408] [arXiv:1502.01518] [INSPIRE].

[9] Y. Bai and T.M.P. Tait, *Searches with Mono-Leptons*, *Phys. Lett. B* **723** (2013) 384 [arXiv:1208.4361] [INSPIRE].

[10] ATLAS collaboration, *Search for dark matter in events with a hadronically decaying W or Z boson and missing transverse momentum in pp collisions at $\sqrt{s} = 8$ TeV with the ATLAS detector*, *Phys. Rev. Lett.* **112** (2014) 041802 [arXiv:1309.4017] [INSPIRE].

[11] CMS collaboration, *Search for physics beyond the standard model in final states with a lepton and missing transverse energy in proton-proton collisions at $\sqrt{s} = 8$ TeV*, *Phys. Rev. D* **91** (2015) 092005 [arXiv:1408.2745] [INSPIRE].

[12] N.F. Bell, A.J. Galea, J.B. Dent, T.D. Jacques, L.M. Krauss and T.J. Weiler, *Searching for Dark Matter at the LHC with a Mono-Z*, *Phys. Rev. D* **86** (2012) 096011 [arXiv:1209.0231] [INSPIRE].

[13] L.M. Carpenter, A. Nelson, C. Shimmin, T.M.P. Tait and D. Whiteson, *Collider searches for dark matter in events with a Z boson and missing energy*, *Phys. Rev. D* **87** (2013) 074005 [arXiv:1212.3352] [INSPIRE].

[14] ATLAS collaboration, *Search for dark matter in events with a Z boson and missing transverse momentum in pp collisions at $\sqrt{s} = 8$ TeV with the ATLAS detector*, Phys. Rev. D **90** (2014) 012004 [arXiv:1404.0051] [INSPIRE].

[15] L. Carpenter, A. DiFranzo, M. Mulhearn, C. Shimmin, S. Tulin and D. Whiteson, *Mono-Higgs-boson: A new collider probe of dark matter*, Phys. Rev. D **89** (2014) 075017 [arXiv:1312.2592] [INSPIRE].

[16] A. Berlin, T. Lin and L.-T. Wang, *Mono-Higgs Detection of Dark Matter at the LHC*, JHEP **06** (2014) 078 [arXiv:1402.7074] [INSPIRE].

[17] CMS collaboration, *Search for new phenomena in monophoton final states in proton-proton collisions at $\sqrt{s} = 8$ TeV*, Phys. Lett. B **755** (2016) 102 [arXiv:1410.8812] [INSPIRE].

[18] ATLAS collaboration, *Search for new phenomena in events with a photon and missing transverse momentum in pp collisions at $\sqrt{s} = 8$ TeV with the ATLAS detector*, Phys. Rev. D **91** (2015) 012008 [*Erratum ibid.* **92** (2015) 059903] [arXiv:1411.1559] [INSPIRE].

[19] CMS collaboration, *Search for new particles in events with energetic jets and large missing transverse momentum in proton-proton collisions at $\sqrt{s} = 13$ TeV*, JHEP **11** (2021) 153 [arXiv:2107.13021] [INSPIRE].

[20] ATLAS collaboration, *Search for new phenomena in events with an energetic jet and missing transverse momentum in pp collisions at $\sqrt{s} = 13$ TeV with the ATLAS detector*, Phys. Rev. D **103** (2021) 112006 [arXiv:2102.10874] [INSPIRE].

[21] CMS collaboration, *Search for dark matter produced in association with a leptonically decaying Z boson in proton-proton collisions at $\sqrt{s} = 13$ TeV*, Eur. Phys. J. C **81** (2021) 13 [*Erratum ibid.* **81** (2021) 333] [arXiv:2008.04735] [INSPIRE].

[22] ATLAS collaboration, *Search for associated production of a Z boson with an invisibly decaying Higgs boson or dark matter candidates at $\sqrt{s} = 13$ TeV with the ATLAS detector*, Phys. Lett. B **829** (2022) 137066 [arXiv:2111.08372] [INSPIRE].

[23] CMS collaboration, *Search for dark matter produced in association with a Higgs boson decaying to a pair of bottom quarks in proton-proton collisions at $\sqrt{s} = 13$ TeV*, Eur. Phys. J. C **79** (2019) 280 [arXiv:1811.06562] [INSPIRE].

[24] CMS collaboration, *Search for dark matter particles produced in association with a Higgs boson in proton-proton collisions at $\sqrt{s} = 13$ TeV*, JHEP **03** (2020) 025 [arXiv:1908.01713] [INSPIRE].

[25] CMS collaboration, *Search for new physics in final states with a single photon and missing transverse momentum in proton-proton collisions at $\sqrt{s} = 13$ TeV*, JHEP **02** (2019) 074 [arXiv:1810.00196] [INSPIRE].

[26] ATLAS collaboration, *Search for dark matter in association with an energetic photon in pp collisions at $\sqrt{s} = 13$ TeV with the ATLAS detector*, JHEP **02** (2021) 226 [arXiv:2011.05259] [INSPIRE].

[27] CMS collaboration, *Search for dark matter in events with energetic, hadronically decaying top quarks and missing transverse momentum at $\sqrt{s} = 13$ TeV*, JHEP **06** (2018) 027 [arXiv:1801.08427] [INSPIRE].

[28] ATLAS collaboration, *Search for new particles in final states with a boosted top quark and missing transverse momentum in proton-proton collisions at $\sqrt{s} = 13$ TeV with the ATLAS detector*, JHEP **05** (2024) 263 [arXiv:2402.16561] [INSPIRE].




JHEP09(2025)141

[29] N. Cabibbo, *Unitary Symmetry and Leptonic Decays*, *Phys. Rev. Lett.* **10** (1963) 531 [INSPIRE].

[30] M. Kobayashi and T. Maskawa, *CP Violation in the Renormalizable Theory of Weak Interaction*, *Prog. Theor. Phys.* **49** (1973) 652 [INSPIRE].

[31] S.L. Glashow, J. Iliopoulos and L. Maiani, *Weak Interactions with Lepton-Hadron Symmetry*, *Phys. Rev. D* **2** (1970) 1285 [INSPIRE].

[32] J. Andrea, B. Fuks and F. Maltoni, *Monotops at the LHC*, *Phys. Rev. D* **84** (2011) 074025 [arXiv:1106.6199] [INSPIRE].

[33] H. Qu and L. Gouskos, *ParticleNet: Jet Tagging via Particle Clouds*, *Phys. Rev. D* **101** (2020) 056019 [arXiv:1902.08570] [INSPIRE].

[34] HEPData record for this analysis, DOI:10.17182/hepdata.156969, (2025).

[35] CMS collaboration, *Performance of the CMS Level-1 trigger in proton-proton collisions at* $\sqrt{s} = 13$ *TeV*, 2020 *JINST* **15** P10017 [arXiv:2006.10165] [INSPIRE].

[36] CMS collaboration, *The CMS trigger system*, 2017 *JINST* **12** P01020 [arXiv:1609.02366] [INSPIRE].

[37] CMS collaboration, *Performance of the CMS high-level trigger during LHC Run 2*, 2024 *JINST* **19** P11021 [arXiv:2410.17038] [INSPIRE].

[38] D. Contardo et al., *Technical Proposal for the Phase-II Upgrade of the CMS Detector*, CERN-LHCC-2015-010 (2015) [INSPIRE].

[39] CMS collaboration, *The CMS Experiment at the CERN LHC*, 2008 *JINST* **3** S08004 [INSPIRE].

[40] CMS collaboration, *Development of the CMS detector for the CERN LHC Run 3*, 2024 *JINST* **19** P05064 [arXiv:2309.05466] [INSPIRE].

[41] CMS collaboration, *Particle-flow reconstruction and global event description with the CMS detector*, 2017 *JINST* **12** P10003 [arXiv:1706.04965] [INSPIRE].

[42] M. Cacciari, G.P. Salam and G. Soyez, *The anti-$k_t$ jet clustering algorithm*, *JHEP* **04** (2008) 063 [arXiv:0802.1189] [INSPIRE].

[43] M. Cacciari, G.P. Salam and G. Soyez, *FastJet User Manual*, *Eur. Phys. J. C* **72** (2012) 1896 [arXiv:1111.6097] [INSPIRE].

[44] CMS collaboration, *Pileup mitigation at CMS in* 13 *TeV data*, 2020 *JINST* **15** P09018 [arXiv:2003.00503] [INSPIRE].

[45] D. Bertolini, P. Harris, M. Low and N. Tran, *Pileup Per Particle Identification*, *JHEP* **10** (2014) 059 [arXiv:1407.6013] [INSPIRE].

[46] CMS collaboration, *Jet energy scale and resolution in the CMS experiment in pp collisions at* 8 *TeV*, 2017 *JINST* **12** P02014 [arXiv:1607.03663] [INSPIRE].

[47] CMS collaboration, *Performance of missing transverse momentum reconstruction in proton-proton collisions at* $\sqrt{s} = 13$ *TeV using the CMS detector*, 2019 *JINST* **14** P07004 [arXiv:1903.06078] [INSPIRE].

[48] CMS collaboration, *Electron and photon reconstruction and identification with the CMS experiment at the CERN LHC*, 2021 *JINST* **16** P05014 [arXiv:2012.06888] [INSPIRE].

[49] CMS collaboration, *Muon identification using multivariate techniques in the CMS experiment in proton-proton collisions at* $\sqrt{s} = 13$ *TeV*, 2024 *JINST* **19** P02031 [arXiv:2310.03844] [INSPIRE].




JHEP09(2025)141

[50] E. Bols, J. Kieseler, M. Verzetti, M. Stoye and A. Stakia, *Jet Flavour Classification Using DeepJet*, 2020 *JINST* **15** P12012 [arXiv:2008.10519] [INSPIRE].

[51] A. Boveia et al., *Recommendations on presenting LHC searches for missing transverse energy signals using simplified s-channel models of dark matter*, *Phys. Dark Univ.* **27** (2020) 100365 [arXiv:1603.04156] [INSPIRE].

[52] A. Albert et al., *Recommendations of the LHC Dark Matter Working Group: Comparing LHC searches for dark matter mediators in visible and invisible decay channels and calculations of the thermal relic density*, *Phys. Dark Univ.* **26** (2019) 100377 [arXiv:1703.05703] [INSPIRE].

[53] T. Sjöstrand et al., *An introduction to PYTHIA 8.2*, *Comput. Phys. Commun.* **191** (2015) 159 [arXiv:1410.3012] [INSPIRE].

[54] J. Alwall et al., *The automated computation of tree-level and next-to-leading order differential cross sections, and their matching to parton shower simulations*, *JHEP* **07** (2014) 079 [arXiv:1405.0301] [INSPIRE].

[55] P. Nason, *A New method for combining NLO QCD with shower Monte Carlo algorithms*, *JHEP* **11** (2004) 040 [hep-ph/0409146] [INSPIRE].

[56] S. Frixione, P. Nason and C. Oleari, *Matching NLO QCD computations with Parton Shower simulations: the POWHEG method*, *JHEP* **11** (2007) 070 [arXiv:0709.2092] [INSPIRE].

[57] S. Alioli, P. Nason, C. Oleari and E. Re, *A general framework for implementing NLO calculations in shower Monte Carlo programs: the POWHEG BOX*, *JHEP* **06** (2010) 043 [arXiv:1002.2581] [INSPIRE].

[58] NNPDF collaboration, *Parton distributions from high-precision collider data*, *Eur. Phys. J. C* **77** (2017) 663 [arXiv:1706.00428] [INSPIRE].

[59] CMS collaboration, *Extraction and validation of a new set of CMS PYTHIA8 tunes from underlying-event measurements*, *Eur. Phys. J. C* **80** (2020) 4 [arXiv:1903.12179] [INSPIRE].

[60] GEANT4 collaboration, *GEANT4 — A Simulation Toolkit*, *Nucl. Instrum. Meth. A* **506** (2003) 250 [INSPIRE].

[61] K. Mawatari, J. Wang, G. Das, C. Degrande, C. Arina and J. Heisig, *DMsimp: Simplified dark matter models*, (2020), https://feynrules.irmp.ucl.ac.be/wiki/DMsimp.

[62] O. Mattelaer, *On the maximal use of Monte Carlo samples: re-weighting events at NLO accuracy*, *Eur. Phys. J. C* **76** (2016) 674 [arXiv:1607.00763] [INSPIRE].

[63] S. Frixione, G. Ridolfi and P. Nason, *A Positive-weight next-to-leading-order Monte Carlo for heavy flavour hadroproduction*, *JHEP* **09** (2007) 126 [arXiv:0707.3088] [INSPIRE].

[64] M. Beneke, P. Falgari, S. Klein and C. Schwinn, *Hadronic top-quark pair production with NNLL threshold resummation*, *Nucl. Phys. B* **855** (2012) 695 [arXiv:1109.1536] [INSPIRE].

[65] M. Cacciari, M. Czakon, M. Mangano, A. Mitov and P. Nason, *Top-pair production at hadron colliders with next-to-next-to-leading logarithmic soft-gluon resummation*, *Phys. Lett. B* **710** (2012) 612 [arXiv:1111.5869] [INSPIRE].

[66] P. Bärnreuther, M. Czakon and A. Mitov, *Percent Level Precision Physics at the Tevatron: First Genuine NNLO QCD Corrections to $q\bar{q} \to t\bar{t} + X$*, *Phys. Rev. Lett.* **109** (2012) 132001 [arXiv:1204.5201] [INSPIRE].

[67] M. Czakon and A. Mitov, *NNLO corrections to top-pair production at hadron colliders: the all-fermionic scattering channels*, *JHEP* **12** (2012) 054 [arXiv:1207.0236] [INSPIRE].


JHEP09(2025)141

[68] M. Czakon and A. Mitov, *NNLO corrections to top pair production at hadron colliders: the quark-gluon reaction*, *JHEP* **01** (2013) 080 [arXiv:1210.6832] [INSPIRE].

[69] M. Czakon, P. Fiedler and A. Mitov, *Total Top-Quark Pair-Production Cross Section at Hadron Colliders Through $O(\alpha_S^4)$*, *Phys. Rev. Lett.* **110** (2013) 252004 [arXiv:1303.6254] [INSPIRE].

[70] M. Czakon and A. Mitov, *Top++: A Program for the Calculation of the Top-Pair Cross-Section at Hadron Colliders*, *Comput. Phys. Commun.* **185** (2014) 2930 [arXiv:1112.5675] [INSPIRE].

[71] S. Alioli, P. Nason, C. Oleari and E. Re, *NLO single-top production matched with shower in POWHEG: s- and t-channel contributions*, *JHEP* **09** (2009) 111 [*Erratum ibid.* **02** (2010) 011] [arXiv:0907.4076] [INSPIRE].

[72] E. Re, *Single-top Wt-channel production matched with parton showers using the POWHEG method*, *Eur. Phys. J. C* **71** (2011) 1547 [arXiv:1009.2450] [INSPIRE].

[73] M. Aliev, H. Lacker, U. Langenfeld, S. Moch, P. Uwer and M. Wiedermann, *HATHOR: HAdronic Top and Heavy quarks crOss section calculatoR*, *Comput. Phys. Commun.* **182** (2011) 1034 [arXiv:1007.1327] [INSPIRE].

[74] P. Kant et al., *HatHor for single top-quark production: Updated predictions and uncertainty estimates for single top-quark production in hadronic collisions*, *Comput. Phys. Commun.* **191** (2015) 74 [arXiv:1406.4403] [INSPIRE].

[75] N. Kidonakis, *Two-loop soft anomalous dimensions for single top quark associated production with a $W^-$ or $H^-$*, *Phys. Rev. D* **82** (2010) 054018 [arXiv:1005.4451] [INSPIRE].

[76] R. Frederix and S. Frixione, *Merging meets matching in MC@NLO*, *JHEP* **12** (2012) 061 [arXiv:1209.6215] [INSPIRE].

[77] J.M. Lindert et al., *Precise predictions for $V+$ jets dark matter backgrounds*, *Eur. Phys. J. C* **77** (2017) 829 [arXiv:1705.04664] [INSPIRE].

[78] T. Gehrmann et al., *$W^+W^-$ Production at Hadron Colliders in Next to Next to Leading Order QCD*, *Phys. Rev. Lett.* **113** (2014) 212001 [arXiv:1408.5243] [INSPIRE].

[79] F. Cascioli et al., *ZZ production at hadron colliders in NNLO QCD*, *Phys. Lett. B* **735** (2014) 311 [arXiv:1405.2219] [INSPIRE].

[80] J.M. Campbell, R.K. Ellis and C. Williams, *Vector Boson Pair Production at the LHC*, *JHEP* **07** (2011) 018 [arXiv:1105.0020] [INSPIRE].

[81] Particle Data Group, *Review of particle physics*, *Phys. Rev. D* **110** (2024) 030001 [INSPIRE].

[82] M. Cacciari and G.P. Salam, *Pileup subtraction using jet areas*, *Phys. Lett. B* **659** (2008) 119 [arXiv:0707.1378] [INSPIRE].

[83] CMS collaboration, *The CMS Statistical Analysis and Combination Tool: Combine*, *Comput. Softw. Big Sci.* **8** (2024) 19 [arXiv:2404.06614] [INSPIRE].

[84] W. Verkerke and D. Kirkby, *The RooFit toolkit for data modeling*, in the proceedings of the *13th International Conference on Computing in High-Enery and Nuclear Physics (CHEP 2003)*, La Jolla, CA, U.S.A., 24–28 March 2003, *eConf C* **0303241** (2003) MOLT007 [physics/0306116] [INSPIRE].

[85] L. Moneta et al., *The RooStats Project*, in the proceedings of the *13th International Workshop on Advanced Computing and Analysis Techniques in Physics Research (ACAT 2010)*, Jaipur, India, 22–27 February 2010, *PoS* **ACAT2010** (2010) 057 [arXiv:1009.1003] [INSPIRE].

[86] A. Buckley et al., *LHAPDF6: parton density access in the LHC precision era*, *Eur. Phys. J. C* **75** (2015) 132 [arXiv:1412.7420] [INSPIRE].




JHEP09(2025)141

[87] J. Butterworth et al., *PDF4LHC recommendations for LHC Run II*, *J. Phys. G* **43** (2016) 023001 [arXiv:1510.03865] [INSPIRE].

[88] CMS collaboration, *Measurement of differential cross sections for top quark pair production using the lepton+jets final state in proton-proton collisions at* 13 *TeV*, *Phys. Rev. D* **95** (2017) 092001 [arXiv:1610.04191] [INSPIRE].

[89] CMS collaboration, *Precision luminosity measurement in proton-proton collisions at* $\sqrt{s} = 13$ *TeV in 2015 and 2016 at CMS*, *Eur. Phys. J. C* **81** (2021) 800 [arXiv:2104.01927] [INSPIRE].

[90] CMS collaboration, *CMS luminosity measurement for the 2017 data-taking period at* $\sqrt{s} = 13$ *TeV*, CMS-PAS-LUM-17-004 (2018).

[91] CMS collaboration, *CMS luminosity measurement for the 2018 data-taking period at* $\sqrt{s} = 13$ *TeV*, CMS-PAS-LUM-18-002 (2019).

[92] CMS collaboration, *Measurement of the inelastic proton-proton cross section at* $\sqrt{s} = 13$ *TeV*, *JHEP* **07** (2018) 161 [arXiv:1802.02613] [INSPIRE].

[93] CMS collaboration, *Jet energy scale and resolution performance with* 13 *TeV data collected by CMS in 2016–2018*, CMS-DP-2020-019 (2020).

[94] CMS collaboration, *Jet energy scale and resolution measurement with Run 2 Legacy Data Collected by CMS at* 13 *TeV*, CMS-DP-2021-033 (2021).

[95] CMS collaboration, *Identification of heavy-flavour jets with the CMS detector in pp collisions at* 13 *TeV*, 2018 *JINST* **13** P05011 [arXiv:1712.07158] [INSPIRE].

[96] R. Barlow and C. Beeston, *Fitting using finite Monte Carlo samples*, *Comput. Phys. Commun.* **77** (1993) 219 [INSPIRE].

[97] R.D. Cousins, *Lectures on Statistics in Theory: Prelude to Statistics in Practice*, arXiv:1807.05996 [INSPIRE].

[98] G. Cowan, K. Cranmer, E. Gross and O. Vitells, *Asymptotic formulae for likelihood-based tests of new physics*, *Eur. Phys. J. C* **71** (2011) 1554 [*Erratum ibid.* **73** (2013) 2501] [arXiv:1007.1727] [INSPIRE].

[99] T. Junk, *Confidence level computation for combining searches with small statistics*, *Nucl. Instrum. Meth. A* **434** (1999) 435 [hep-ex/9902006] [INSPIRE].

[100] A.L. Read, *Presentation of search results: The* $CL_s$ *technique*, *J. Phys. G* **28** (2002) 2693 [INSPIRE].

[101] M. Backovic, K. Kong and M. McCaskey, *MadDM v.1.0: Computation of Dark Matter Relic Abundance Using MadGraph5*, *Phys. Dark Univ.* **5–6** (2014) 18 [arXiv:1308.4955] [INSPIRE].

[102] F. Ambrogi et al., *MadDM v.3.0: a Comprehensive Tool for Dark Matter Studies*, *Phys. Dark Univ.* **24** (2019) 100249 [arXiv:1804.00044] [INSPIRE].

JHEP09(2025)141

## The CMS collaboration


**Yerevan Physics Institute, Yerevan, Armenia**
V. Chekhovsky, A. Hayrapetyan, V. Makarenko, A. Tumasyan[1]

**Institut für Hochenergiephysik, Vienna, Austria**
W. Adam, J.W. Andrejkovic, L. Benato, T. Bergauer, S. Chatterjee, K. Damanakis, M. Dragicevic, P.S. Hussain, M. Jeitler[2], N. Krammer, A. Li, D. Liko, I. Mikulec, J. Schieck[2], R. Schöfbeck[2], D. Schwarz, M. Sonawane, W. Waltenberger, C.-E. Wulz[2]

**Universiteit Antwerpen, Antwerpen, Belgium**
T. Janssen, H. Kwon, T. Van Laer, P. Van Mechelen

**Vrije Universiteit Brussel, Brussel, Belgium**
N. Breugelmans, J. D'Hondt, S. Dansana, A. De Moor, M. Delcourt, F. Heyen, Y. Hong, S. Lowette, I. Makarenko, D. Müller, S. Tavernier, M. Tytgat[3], G.P. Van Onsem, S. Van Putte, D. Vannerom

**Université Libre de Bruxelles, Bruxelles, Belgium**
B. Bilin, B. Clerbaux, A.K. Das, I. De Bruyn, G. De Lentdecker, H. Evard, L. Favart, P. Gianneios, A. Khalilzadeh, F.A. Khan, A. Malara, M.A. Shahzad, L. Thomas, M. Vanden Bemden, C. Vander Velde, P. Vanlaer

**Ghent University, Ghent, Belgium**
M. De Coen, D. Dobur, G. Gokbulut, J. Knolle, L. Lambrecht, D. Marckx, K. Skovpen, N. Van Den Bossche, J. van der Linden, J. Vandenbroeck, L. Wezenbeek

**Université Catholique de Louvain, Louvain-la-Neuve, Belgium**
S. Bein, A. Benecke, A. Bethani, G. Bruno, C. Caputo, J. De Favereau De Jeneret, C. Delaere, I.S. Donertas, A. Giammanco, A.O. Guzel, Sa. Jain, V. Lemaitre, J. Lidrych, P. Mastrapasqua, T.T. Tran, S. Turkcapar

**Centro Brasileiro de Pesquisas Fisicas, Rio de Janeiro, Brazil**
G.A. Alves, E. Coelho, G. Correia Silva, C. Hensel, T. Menezes De Oliveira, C. Mora Herrera[4], P. Rebello Teles, M. Soeiro, E.J. Tonelli Manganote[5], A. Vilela Pereira[4]

**Universidade do Estado do Rio de Janeiro, Rio de Janeiro, Brazil**
W.L. Aldá Júnior, M. Barroso Ferreira Filho, H. Brandao Malbouisson, W. Carvalho, J. Chinellato[6], E.M. Da Costa, G.G. Da Silveira[7], D. De Jesus Damiao, S. Fonseca De Souza, R. Gomes De Souza, T. Laux Kuhn[7], M. Macedo, K. Mota Amarilo, L. Mundim, H. Nogima, J.P. Pinheiro, A. Santoro, A. Sznajder, M. Thiel

**Universidade Estadual Paulista, Universidade Federal do ABC, São Paulo, Brazil**
C.A. Bernardes[7], L. Calligaris, T.R. Fernandez Perez Tomei, E.M. Gregores, I. Maietto Silverio, P.G. Mercadante, S.F. Novaes, B. Orzari, Sandra S. Padula, V. Scheurer


JHEP09(2025)141

**Institute for Nuclear Research and Nuclear Energy, Bulgarian Academy of Sciences, Sofia, Bulgaria**
A. Aleksandrov, G. Antchev, R. Hadjiiska, P. Iaydjiev, M. Misheva, M. Shopova, G. Sultanov

**University of Sofia, Sofia, Bulgaria**
A. Dimitrov, L. Litov, B. Pavlov, P. Petkov, A. Petrov, E. Shumka

**Instituto De Alta Investigación, Universidad de Tarapacá, Casilla 7 D, Arica, Chile**
S. Keshri, D. Laroze, S. Thakur

**Beihang University, Beijing, China**
T. Cheng, T. Javaid, L. Yuan

**Department of Physics, Tsinghua University, Beijing, China**
Z. Hu, Z. Liang, J. Liu

**Institute of High Energy Physics, Beijing, China**
G.M. Chen[8], H.S. Chen[8], M. Chen[8], F. Iemmi, C.H. Jiang, A. Kapoor[9], H. Liao, Z.-A. Liu[10], R. Sharma[11], J.N. Song[10], J. Tao, C. Wang[8], J. Wang, Z. Wang[8], H. Zhang, J. Zhao

**State Key Laboratory of Nuclear Physics and Technology, Peking University, Beijing, China**
A. Agapitos, Y. Ban, A. Carvalho Antunes De Oliveira, S. Deng, B. Guo, C. Jiang, A. Levin, C. Li, Q. Li, Y. Mao, S. Qian, S.J. Qian, X. Qin, X. Sun, D. Wang, H. Yang, Y. Zhao, C. Zhou

**Guangdong Provincial Key Laboratory of Nuclear Science and Guangdong-Hong Kong Joint Laboratory of Quantum Matter, South China Normal University, Guangzhou, China**
S. Yang

**Sun Yat-Sen University, Guangzhou, China**
Z. You

**University of Science and Technology of China, Hefei, China**
K. Jaffel, N. Lu

**Nanjing Normal University, Nanjing, China**
G. Bauer[12], B. Li[13], H. Wang, K. Yi[14], J. Zhang

**Institute of Modern Physics and Key Laboratory of Nuclear Physics and Ion-beam Application (MOE) - Fudan University, Shanghai, China**
Y. Li



JHEP09(2025)141

**Zhejiang University, Hangzhou, Zhejiang, China**
Z. Lin, C. Lu, M. Xiao

**Universidad de Los Andes, Bogota, Colombia**
C. Avila, D.A. Barbosa Trujillo, A. Cabrera, C. Florez, J. Fraga, J.A. Reyes Vega

**Universidad de Antioquia, Medellin, Colombia**
J. Jaramillo, C. Rendón, M. Rodriguez, A.A. Ruales Barbosa, J.D. Ruiz Alvarez

**University of Split, Faculty of Electrical Engineering, Mechanical Engineering and Naval Architecture, Split, Croatia**
D. Giljanovic, N. Godinovic, D. Lelas, A. Sculac

**University of Split, Faculty of Science, Split, Croatia**
M. Kovac, A. Petkovic, T. Sculac

**Institute Rudjer Boskovic, Zagreb, Croatia**
P. Bargassa, V. Brigljevic, B.K. Chitroda, D. Ferencek, K. Jakovcic, A. Starodumov, T. Susa

**University of Cyprus, Nicosia, Cyprus**
A. Attikis, K. Christoforou, A. Hadjiagapiou, C. Leonidou, J. Mousa, C. Nicolaou, L. Paizanos, F. Ptochos, P.A. Razis, H. Rykaczewski, H. Saka, A. Stepennov

**Charles University, Prague, Czech Republic**
M. Finger, M. Finger Jr., A. Kveton

**Escuela Politecnica Nacional, Quito, Ecuador**
E. Ayala

**Universidad San Francisco de Quito, Quito, Ecuador**
E. Carrera Jarrin

**Academy of Scientific Research and Technology of the Arab Republic of Egypt, Egyptian Network of High Energy Physics, Cairo, Egypt**
B. El-mahdy, S. Khalil[15], E. Salama[16,17]

**Center for High Energy Physics (CHEP-FU), Fayoum University, El-Fayoum, Egypt**
M. Abdullah Al-Mashad, M.A. Mahmoud

**National Institute of Chemical Physics and Biophysics, Tallinn, Estonia**
K. Ehataht, M. Kadastik, T. Lange, C. Nielsen, J. Pata, M. Raidal, L. Tani, C. Veelken

**Department of Physics, University of Helsinki, Helsinki, Finland**
K. Osterberg, M. Voutilainen

JHEP09(2025)141

**Helsinki Institute of Physics, Helsinki, Finland**

N. Bin Norjoharuddeen, E. Brücken, F. Garcia, P. Inkaew, K.T.S. Kallonen, T. Lampén, K. Lassila-Perini, S. Lehti, T. Lindén, M. Myllymäki, M.m. Rantanen, J. Tuominiemi

**Lappeenranta-Lahti University of Technology, Lappeenranta, Finland**

H. Kirschenmann, P. Luukka, H. Petrow

**IRFU, CEA, Université Paris-Saclay, Gif-sur-Yvette, France**

M. Besancon, F. Couderc, M. Dejardin, D. Denegri, J.L. Faure, F. Ferri, S. Ganjour, P. Gras, G. Hamel de Monchenault, M. Kumar, V. Lohezic, J. Malcles, F. Orlandi, L. Portales, A. Rosowsky, M.Ö. Sahin, A. Savoy-Navarro[18], P. Simkina, M. Titov, M. Tornago

**Laboratoire Leprince-Ringuet, CNRS/IN2P3, Ecole Polytechnique, Institut Polytechnique de Paris, Palaiseau, France**

F. Beaudette, G. Boldrini, P. Busson, A. Cappati, C. Charlot, M. Chiusi, T.D. Cuisset, F. Damas, O. Davignon, A. De Wit, I.T. Ehle, B.A. Fontana Santos Alves, S. Ghosh, A. Gilbert, R. Granier de Cassagnac, B. Harikrishnan, L. Kalipoliti, G. Liu, M. Manoni, M. Nguyen, S. Obraztsov, C. Ochando, R. Salerno, J.B. Sauvan, Y. Sirois, G. Sokmen, L. Urda Gómez, E. Vernazza, A. Zabi, A. Zghiche

**Université de Strasbourg, CNRS, IPHC UMR 7178, Strasbourg, France**

J.-L. Agram[19], J. Andrea, D. Bloch, J.-M. Brom, E.C. Chabert, C. Collard, S. Falke, U. Goerlach, R. Haeberle, A.-C. Le Bihan, M. Meena, O. Poncet, G. Saha, M.A. Sessini, P. Van Hove, P. Vaucelle

**Centre de Calcul de l'Institut National de Physique Nucleaire et de Physique des Particules, CNRS/IN2P3, Villeurbanne, France**

A. Di Florio

**Institut de Physique des 2 Infinis de Lyon (IP2I), Villeurbanne, France**

D. Amram, S. Beauceron, B. Blancon, G. Boudoul, N. Chanon, D. Contardo, P. Depasse, C. Dozen[20], H. El Mamouni, J. Fay, S. Gascon, M. Gouzevitch, C. Greenberg, G. Grenier, B. Ille, E. Jourd'huy, I.B. Laktineh, M. Lethuillier, L. Mirabito, S. Perries, A. Purohit, M. Vander Donckt, P. Verdier, J. Xiao

**Georgian Technical University, Tbilisi, Georgia**

A. Khvedelidze[21], I. Lomidze, Z. Tsamalaidze[21]

**RWTH Aachen University, I. Physikalisches Institut, Aachen, Germany**

V. Botta, S. Consuegra Rodríguez, L. Feld, K. Klein, M. Lipinski, D. Meuser, A. Pauls, D. Pérez Adán, N. Röwert, M. Teroerde

**RWTH Aachen University, III. Physikalisches Institut A, Aachen, Germany**

S. Diekmann, A. Dodonova, N. Eich, D. Eliseev, F. Engelke, J. Erdmann, M. Erdmann, B. Fischer, T. Hebbeker, K. Hoepfner, F. Ivone, A. Jung, N. Kumar,




JHEP09(2025)141

M.y. Lee, F. Mausolf, M. Merschmeyer, A. Meyer, F. Nowotny, A. Pozdnyakov, Y. Rath, W. Redjeb, F. Rehm, H. Reithler, V. Sarkisovi, A. Schmidt, C. Seth, A. Sharma, J.L. Spah, F. Torres Da Silva De Araujo[22], S. Wiedenbeck, S. Zaleski

**RWTH Aachen University, III. Physikalisches Institut B, Aachen, Germany**
C. Dziwok, G. Flügge, T. Kress, A. Nowack, O. Pooth, A. Stahl, T. Ziemons, A. Zotz

**Deutsches Elektronen-Synchrotron, Hamburg, Germany**
H. Aarup Petersen, M. Aldaya Martin, J. Alimena, S. Amoroso, Y. An, J. Bach, S. Baxter, M. Bayatmakou, H. Becerril Gonzalez, O. Behnke, A. Belvedere, F. Blekman[23], K. Borras[24], A. Campbell, A. Cardini, F. Colombina, M. De Silva, G. Eckerlin, D. Eckstein, L.I. Estevez Banos, E. Gallo[23], A. Geiser, V. Guglielmi, M. Guthoff, A. Hinzmann, L. Jeppe, B. Kaech, M. Kasemann, C. Kleinwort, R. Kogler, M. Komm, D. Krücker, W. Lange, D. Leyva Pernia, K. Lipka[25], W. Lohmann[26], F. Lorkowski, R. Mankel, I.-A. Melzer-Pellmann, M. Mendizabal Morentin, A.B. Meyer, G. Milella, K. Moral Figueroa, A. Mussgiller, L.P. Nair, J. Niedziela, A. Nürnberg, J. Park, E. Ranken, A. Raspereza, D. Rastorguev, J. Rübenach, L. Rygaard, M. Scham[27,24], S. Schnake[24], P. Schütze, C. Schwanenberger[23], D. Selivanova, K. Sharko, M. Shchedrolosiev, D. Stafford, F. Vazzoler, A. Ventura Barroso, R. Walsh, D. Wang, Q. Wang, K. Wichmann, L. Wiens[24], C. Wissing, Y. Yang, S. Zakharov, A. Zimermmane Castro Santos

**University of Hamburg, Hamburg, Germany**
A. Albrecht, S. Albrecht, M. Antonello, S. Bollweg, M. Bonanomi, P. Connor, K. El Morabit, Y. Fischer, E. Garutti, A. Grohsjean, J. Haller, D. Hundhausen, H.R. Jabusch, G. Kasieczka, P. Keicher, R. Klanner, W. Korcari, T. Kramer, C.c. Kuo, V. Kutzner, F. Labe, J. Lange, A. Lobanov, C. Matthies, L. Moureaux, M. Mrowietz, A. Nigamova, Y. Nissan, A. Paasch, K.J. Pena Rodriguez, T. Quadfasel, B. Raciti, M. Rieger, D. Savoiu, J. Schindler, P. Schleper, M. Schröder, J. Schwandt, M. Sommerhalder, H. Stadie, G. Steinbrück, A. Tews, B. Wiederspan, M. Wolf

**Karlsruher Institut fuer Technologie, Karlsruhe, Germany**
S. Brommer, E. Butz, Y.M. Chen, T. Chwalek, A. Dierlamm, G.G. Dincer, U. Elicabuk, N. Faltermann, M. Giffels, A. Gottmann, F. Hartmann[28], R. Hofsaess, M. Horzela, U. Husemann, J. Kieseler, M. Klute, O. Lavoryk, J.M. Lawhorn, M. Link, A. Lintuluoto, S. Maier, M. Molch, M. Mormile, Th. Müller, M. Neukum, M. Oh, E. Pfeffer, M. Presilla, G. Quast, K. Rabbertz, B. Regnery, R. Schmieder, N. Shadskiy, I. Shvetsov, H.J. Simonis, L. Sowa, L. Stockmeier, K. Tauqeer, M. Toms, B. Topko, N. Trevisani, T. Voigtländer, R.F. Von Cube, J. Von Den Driesch, M. Wassmer, S. Wieland, F. Wittig, R. Wolf, X. Zuo

**Institute of Nuclear and Particle Physics (INPP), NCSR Demokritos, Aghia Paraskevi, Greece**
G. Anagnostou, G. Daskalakis, A. Kyriakis, A. Papadopoulos[28], A. Stakia

**National and Kapodistrian University of Athens, Athens, Greece**
G. Melachroinos, Z. Painesis, I. Paraskevas, N. Saoulidou, K. Theofilatos, E. Tziaferi, K. Vellidis, I. Zisopoulos

**National Technical University of Athens, Athens, Greece**
G. Bakas, T. Chatzistavrou, G. Karapostoli, K. Kousouris, I. Papakrivopoulos, E. Siamarkou, G. Tsipolitis

**University of Ioánnina, Ioánnina, Greece**
I. Bestintzanos, I. Evangelou, C. Foudas, C. Kamtsikis, P. Katsoulis, P. Kokkas, P.G. Kosmoglou Kioseoglou, N. Manthos, I. Papadopoulos, J. Strologas

**HUN-REN Wigner Research Centre for Physics, Budapest, Hungary**
C. Hajdu, D. Horvath[29,30], K. Márton, A.J. Rádl[31], F. Sikler, V. Veszpremi

**MTA-ELTE Lendület CMS Particle and Nuclear Physics Group, Eötvös Loránd University, Budapest, Hungary**
M. Csanád, K. Farkas, A. Fehérkuti[32], M.M.A. Gadallah[33], Á. Kadlecsik, G. Pásztor, G.I. Veres

**Faculty of Informatics, University of Debrecen, Debrecen, Hungary**
B. Ujvari, G. Zilizi

**HUN-REN ATOMKI - Institute of Nuclear Research, Debrecen, Hungary**
G. Bencze, S. Czellar, J. Molnar, Z. Szillasi

**Karoly Robert Campus, MATE Institute of Technology, Gyongyos, Hungary**
T. Csorgo[32], F. Nemes[32], T. Novak

**Panjab University, Chandigarh, India**
S. Bansal, S.B. Beri, V. Bhatnagar, G. Chaudhary, S. Chauhan, N. Dhingra[34], A. Kaur, A. Kaur, H. Kaur, M. Kaur, S. Kumar, T. Sheokand, J.B. Singh, A. Singla

**University of Delhi, Delhi, India**
A. Bhardwaj, A. Chhetri, B.C. Choudhary, A. Kumar, A. Kumar, M. Naimuddin, K. Ranjan, M.K. Saini, S. Saumya

**Indian Institute of Technology Kanpur, Kanpur, India**
S. Mukherjee

**Saha Institute of Nuclear Physics, HBNI, Kolkata, India**
S. Baradia, S. Barman[35], S. Bhattacharya, S. Das Gupta, S. Dutta, S. Dutta, S. Sarkar

**Indian Institute of Technology Madras, Madras, India**
M.M. Ameen, P.K. Behera, S.C. Behera, S. Chatterjee, G. Dash, P. Jana, P. Kalbhor, S. Kamble, J.R. Komaragiri[36], D. Kumar[36], T. Mishra, B. Parida[37], P.R. Pujahari, N.R. Saha, A.K. Sikdar, R.K. Singh, P. Verma, S. Verma, A. Vijay

JHEP09(2025)141

**Tata Institute of Fundamental Research-A, Mumbai, India**
S. Dugad, G.B. Mohanty, M. Shelake, P. Suryadevara

**Tata Institute of Fundamental Research-B, Mumbai, India**
A. Bala, S. Banerjee, S. Bhowmik[38], R.M. Chatterjee, M. Guchait, Sh. Jain, A. Jaiswal, B.M. Joshi, S. Kumar, G. Majumder, K. Mazumdar, S. Parolia, A. Thachayath

**National Institute of Science Education and Research, An OCC of Homi Bhabha National Institute, Bhubaneswar, Odisha, India**
S. Bahinipati[39], C. Kar, D. Maity[40], P. Mal, K. Naskar[40], A. Nayak[40], S. Nayak, K. Pal, R. Raturi, P. Sadangi, S.K. Swain, S. Varghese[40], D. Vats[40]

**Indian Institute of Science Education and Research (IISER), Pune, India**
S. Acharya[41], A. Alpana, S. Dube, B. Gomber[41], P. Hazarika, B. Kansal, A. Laha, B. Sahu[41], S. Sharma, K.Y. Vaish

**Isfahan University of Technology, Isfahan, Iran**
H. Bakhshiansohi[42], A. Jafari[42], M. Zeinali[43]

**Institute for Research in Fundamental Sciences (IPM), Tehran, Iran**
S. Bashiri, S. Chenarani[44], S.M. Etesami, Y. Hosseini, M. Khakzad, E. Khazaie, M. Mohammadi Najafabadi, S. Tizchang[45]

**University College Dublin, Dublin, Ireland**
M. Felcini, M. Grunewald

**INFN Sezione di Bari[a], Università di Bari[b], Politecnico di Bari[c], Bari, Italy**
M. Abbrescia[a,b], A. Colaleo[a,b], D. Creanza[a,c], B. D'Anzi[a,b], N. De Filippis[a,c], M. De Palma[a,b], W. Elmetenawee[a,b,46], N. Ferrara[a,b], L. Fiore[a], G. Iaselli[a,c], L. Longo[a], M. Louka[a,b], G. Maggi[a,c], M. Maggi[a], I. Margjeka[a], V. Mastrapasqua[a,b], S. My[a,b], S. Nuzzo[a,b], A. Pellecchia[a,b], A. Pompili[a,b], G. Pugliese[a,c], R. Radogna[a,b], D. Ramos[a], A. Ranieri[a], L. Silvestris[a], F.M. Simone[a,c], Ü. Sözbilir[a], A. Stamerra[a,b], D. Troiano[a,b], R. Venditti[a,b], P. Verwilligen[a], A. Zaza[a,b]

**INFN Sezione di Bologna[a], Università di Bologna[b], Bologna, Italy**
G. Abbiendi[a], C. Battilana[a,b], D. Bonacorsi[a,b], P. Capiluppi[a,b], A. Castro[†,a,b], F.R. Cavallo[a], M. Cuffiani[a,b], G.M. Dallavalle[a], T. Diotalevi[a,b], F. Fabbri[a], A. Fanfani[a,b], D. Fasanella[a], P. Giacomelli[a], L. Giommi[a,b], C. Grandi[a], L. Guiducci[a,b], S. Lo Meo[a,47], M. Lorusso[a,b], L. Lunerti[a], S. Marcellini[a], G. Masetti[a], F.L. Navarria[a,b], G. Paggi[a,b], A. Perrotta[a], F. Primavera[a,b], A.M. Rossi[a,b], S. Rossi Tisbeni[a,b], T. Rovelli[a,b], G.P. Siroli[a,b]

**INFN Sezione di Catania[a], Università di Catania[b], Catania, Italy**
S. Costa[a,b,48], A. Di Mattia[a], A. Lapertosa[a], R. Potenza[a,b], A. Tricomi[a,b,48]



JHEP09(2025)141

**INFN Sezione di Firenze[a], Università di Firenze[b], Firenze, Italy**

P. Assiouras[a], G. Barbagli[a], G. Bardelli[a,b], M. Bartolini[a,b], B. Camaiani[a,b], A. Cassese[a], R. Ceccarelli[a], V. Ciulli[a,b], C. Civinini[a], R. D'Alessandro[a,b], L. Damenti[a,b], E. Focardi[a,b], T. Kello[a], G. Latino[a,b], P. Lenzi[a,b], M. Lizzo[a], M. Meschini[a], S. Paoletti[a], A. Papanastassiou[a,b], G. Sguazzoni[a], L. Viliani[a]

**INFN Laboratori Nazionali di Frascati, Frascati, Italy**

L. Benussi, S. Bianco, S. Meola[49], D. Piccolo

**INFN Sezione di Genova[a], Università di Genova[b], Genova, Italy**

M. Alves Gallo Pereira[a], F. Ferro[a], E. Robutti[a], S. Tosi[a,b]

**INFN Sezione di Milano-Bicocca[a], Università di Milano-Bicocca[b], Milano, Italy**

A. Benaglia[a], F. Brivio[a], F. Cetorelli[a,b], F. De Guio[a,b], M.E. Dinardo[a,b], P. Dini[a], S. Gennai[a], R. Gerosa[a,b], A. Ghezzi[a,b], P. Govoni[a,b], L. Guzzi[a], G. Lavizzari[a,b], M.T. Lucchini[a,b], M. Malberti[a], S. Malvezzi[a], A. Massironi[a], D. Menasce[a], L. Moroni[a], M. Paganoni[a,b], S. Palluotto[a,b], D. Pedrini[a], A. Perego[a,b], B.S. Pinolini[a], G. Pizzati[a,b], S. Ragazzi[a,b], T. Tabarelli de Fatis[a,b]

**INFN Sezione di Napoli[a], Università di Napoli 'Federico II'[b], Napoli, Italy; Università della Basilicata[c], Potenza, Italy; Scuola Superiore Meridionale (SSM)[d], Napoli, Italy**

S. Buontempo[a], A. Cagnotta[a,b], F. Carnevali[a,b], N. Cavallo[a,c], F. Fabozzi[a,c], A.O.M. Iorio[a,b], L. Lista[a,b,50], P. Paolucci[a,28], B. Rossi[a]

**INFN Sezione di Padova[a], Università di Padova[b], Padova, Italy; Università di Trento[c], Trento, Italy**

R. Ardino[a], P. Azzi[a], N. Bacchetta[a,51], M. Biasotto[a,52], D. Bisello[a,b], P. Bortignon[a], G. Bortolato[a,b], A.C.M. Bulla[a], R. Carlin[a,b], P. Checchia[a], T. Dorigo[a,53], F. Gasparini[a,b], U. Gasparini[a,b], S. Giorgetti[a], E. Lusiani[a], M. Margoni[a,b], A.T. Meneguzzo[a,b], J. Pazzini[a,b], P. Ronchese[a,b], R. Rossin[a,b], F. Simonetto[a,b], M. Tosi[a,b], A. Triossi[a,b], S. Ventura[a], P. Zotto[a,b], A. Zucchetta[a,b], G. Zumerle[a,b]

**INFN Sezione di Pavia[a], Università di Pavia[b], Pavia, Italy**

A. Braghieri[a], S. Calzaferri[a], D. Fiorina[a], P. Montagna[a,b], M. Pelliccioni[a], V. Re[a], C. Riccardi[a,b], P. Salvini[a], I. Vai[a,b], P. Vitulo[a,b]

**INFN Sezione di Perugia[a], Università di Perugia[b], Perugia, Italy**

S. Ajmal[a,b], M.E. Ascioti[a,b], G.M. Bilei[a], C. Carrivale[a,b], D. Ciangottini[a,b], L. Fanò[a,b], V. Mariani[a,b], M. Menichelli[a], F. Moscatelli[a,54], A. Rossi[a,b], A. Santocchia[a,b], D. Spiga[a], T. Tedeschi[a,b]

**INFN Sezione di Pisa[a], Università di Pisa[b], Scuola Normale Superiore di Pisa[c], Pisa, Italy; Università di Siena[d], Siena, Italy**

C. Aimè[a], C.A. Alexe[a,c], P. Asenov[a,b], P. Azzurri[a], G. Bagliesi[a], R. Bhattacharya[a], L. Bianchini[a,b], T. Boccali[a], E. Bossini[a], D. Bruschini[a,c], R. Castaldi[a], F. Cattafesta[a,c],

JHEP09(2025)141

M.A. Ciocci[a,b], M. Cipriani[a,b], V. D'Amante[a,d], R. Dell'Orso[a], S. Donato[a,b], A. Giassi[a], F. Ligabue[a,c], A.C. Marini[a,b], D. Matos Figueiredo[a], A. Messineo[a,b], S. Mishra[a], V.K. Muraleedharan Nair Bindhu[a,b,40], M. Musich[a,b], S. Nandan[a], F. Palla[a], A. Rizzi[a,b], G. Rolandi[a,c], S. Roy Chowdhury[a,38], T. Sarkar[a], A. Scribano[a], P. Spagnolo[a], F. Tenchini[a,b], R. Tenchini[a], G. Tonelli[a,b], N. Turini[a,d], F. Vaselli[a,c], A. Venturi[a], P.G. Verdini[a]

**INFN Sezione di Roma[a], Sapienza Università di Roma[b], Roma, Italy**

P. Barria[a], C. Basile[a,b], F. Cavallari[a], L. Cunqueiro Mendez[a,b], D. Del Re[a,b], E. Di Marco[a,b], M. Diemoz[a], F. Errico[a,b], R. Gargiulo[a,b], E. Longo[a,b], L. Martikainen[a,b], J. Mijuskovic[a,b], G. Organtini[a,b], F. Pandolfi[a], R. Paramatti[a,b], C. Quaranta[a,b], S. Rahatlou[a,b], C. Rovelli[a], F. Santanastasio[a,b], L. Soffi[a], V. Vladimirov[a,b]

**INFN Sezione di Torino[a], Università di Torino[b], Torino, Italy; Università del Piemonte Orientale[c], Novara, Italy**

N. Amapane[a,b], R. Arcidiacono[a,c], S. Argiro[a,b], M. Arneodo[a,c], N. Bartosik[a,c], R. Bellan[a,b], C. Biino[a], C. Borca[a,b], N. Cartiglia[a], M. Costa[a,b], R. Covarelli[a,b], N. Demaria[a], L. Finco[a], M. Grippo[a,b], B. Kiani[a,b], F. Legger[a], F. Luongo[a,b], C. Mariotti[a], L. Markovic[a,b], S. Maselli[a], A. Mecca[a,b], L. Menzio[a,b], P. Meridiani[a], E. Migliore[a,b], M. Monteno[a], R. Mulargia[a], M.M. Obertino[a,b], G. Ortona[a], L. Pacher[a,b], N. Pastrone[a], M. Ruspa[a,c], F. Siviero[a,b], V. Sola[a,b], A. Solano[a,b], A. Staiano[a], C. Tarricone[a,b], D. Trocino[a], G. Umoret[a,b], R. White[a,b]

**INFN Sezione di Trieste[a], Università di Trieste[b], Trieste, Italy**

J. Babbar[a,b], S. Belforte[a], V. Candelise[a,b], M. Casarsa[a], F. Cossutti[a], K. De Leo[a], G. Della Ricca[a,b]

**Kyungpook National University, Daegu, Korea**

S. Dogra, J. Hong, J. Kim, D. Lee, H. Lee, S.W. Lee, C.S. Moon, Y.D. Oh, M.S. Ryu, S. Sekmen, B. Tae, Y.C. Yang

**Department of Mathematics and Physics - GWNU, Gangneung, Korea**

M.S. Kim

**Chonnam National University, Institute for Universe and Elementary Particles, Kwangju, Korea**

G. Bak, P. Gwak, H. Kim, D.H. Moon

**Hanyang University, Seoul, Korea**

E. Asilar, J. Choi[55], D. Kim, T.J. Kim, J.A. Merlin, Y. Ryou

**Korea University, Seoul, Korea**

S. Choi, S. Han, B. Hong, K. Lee, K.S. Lee, S. Lee, J. Yoo

**Kyung Hee University, Department of Physics, Seoul, Korea**

J. Goh, S. Yang

JHEP09(2025)141

**Sejong University, Seoul, Korea**
Y. Kang, H.S. Kim, Y. Kim, S. Lee

**Seoul National University, Seoul, Korea**
J. Almond, J.H. Bhyun, J. Choi, J. Choi, W. Jun, J. Kim, Y.W. Kim, S. Ko, H. Lee, J. Lee, J. Lee, B.H. Oh, S.B. Oh, H. Seo, U.K. Yang, I. Yoon

**University of Seoul, Seoul, Korea**
W. Jang, D.Y. Kang, S. Kim, B. Ko, J.S.H. Lee, Y. Lee, I.C. Park, Y. Roh, I.J. Watson

**Yonsei University, Department of Physics, Seoul, Korea**
S. Ha, K. Hwang, B. Kim, K. Lee, H.D. Yoo

**Sungkyunkwan University, Suwon, Korea**
M. Choi, M.R. Kim, H. Lee, Y. Lee, I. Yu

**College of Engineering and Technology, American University of the Middle East (AUM), Dasman, Kuwait**
T. Beyrouthy, Y. Gharbia

**Kuwait University - College of Science - Department of Physics, Safat, Kuwait**
F. Alazemi

**Riga Technical University, Riga, Latvia**
K. Dreimanis, A. Gaile, C. Munoz Diaz, D. Osite, G. Pikurs, A. Potrebko, M. Seidel, D. Sidiropoulos Kontos

**University of Latvia (LU), Riga, Latvia**
N.R. Strautnieks

**Vilnius University, Vilnius, Lithuania**
M. Ambrozas, A. Juodagalvis, A. Rinkevicius, G. Tamulaitis

**National Centre for Particle Physics, Universiti Malaya, Kuala Lumpur, Malaysia**
I. Yusuff[56], Z. Zolkapli

**Universidad de Sonora (UNISON), Hermosillo, Mexico**
J.F. Benitez, A. Castaneda Hernandez, H.A. Encinas Acosta, L.G. Gallegos Maríñez, M. León Coello, J.A. Murillo Quijada, A. Sehrawat, L. Valencia Palomo

**Centro de Investigacion y de Estudios Avanzados del IPN, Mexico City, Mexico**
G. Ayala, H. Castilla-Valdez, H. Crotte Ledesma, E. De La Cruz-Burelo, I. Heredia-De La Cruz[57], R. Lopez-Fernandez, J. Mejia Guisao, A. Sánchez Hernández

**Universidad Iberoamericana, Mexico City, Mexico**
C. Oropeza Barrera, D.L. Ramirez Guadarrama, M. Ramírez García



JHEP09(2025)141

**Benemerita Universidad Autonoma de Puebla, Puebla, Mexico**
I. Bautista, F.E. Neri Huerta, I. Pedraza, H.A. Salazar Ibarguen, C. Uribe Estrada

**University of Montenegro, Podgorica, Montenegro**
I. Bubanja, N. Raicevic

**University of Canterbury, Christchurch, New Zealand**
P.H. Butler

**National Centre for Physics, Quaid-I-Azam University, Islamabad, Pakistan**
A. Ahmad, M.I. Asghar, A. Awais, M.I.M. Awan, H.R. Hoorani, W.A. Khan

**AGH University of Krakow, Krakow, Poland**
V. Avati, A. Bellora[58], L. Forthomme, L. Grzanka, M. Malawski, K. Piotrzkowski

**National Centre for Nuclear Research, Swierk, Poland**
H. Bialkowska, M. Bluj, M. Górski, M. Kazana, M. Szleper, P. Zalewski

**Institute of Experimental Physics, Faculty of Physics, University of Warsaw, Warsaw, Poland**
K. Bunkowski, K. Doroba, A. Kalinowski, M. Konecki, J. Krolikowski, A. Muhammad

**Warsaw University of Technology, Warsaw, Poland**
P. Fokow, K. Pozniak, W. Zabolotny

**Laboratório de Instrumentação e Física Experimental de Partículas, Lisboa, Portugal**
M. Araujo, D. Bastos, C. Beirão Da Cruz E. Silva, A. Boletti, M. Bozzo, T. Camporesi, G. Da Molin, P. Faccioli, M. Gallinaro, J. Hollar, N. Leonardo, G.B. Marozzo, A. Petrilli, M. Pisano, J. Seixas, J. Varela, J.W. Wulff

**Faculty of Physics, University of Belgrade, Belgrade, Serbia**
P. Adzic, P. Milenovic

**VINCA Institute of Nuclear Sciences, University of Belgrade, Belgrade, Serbia**
D. Devetak, M. Dordevic, J. Milosevic, L. Nadderd, V. Rekovic, M. Stojanovic

**Centro de Investigaciones Energéticas Medioambientales y Tecnológicas (CIEMAT), Madrid, Spain**
J. Alcaraz Maestre, Cristina F. Bedoya, J.A. Brochero Cifuentes, Oliver M. Carretero, M. Cepeda, M. Cerrada, N. Colino, B. De La Cruz, A. Delgado Peris, A. Escalante Del Valle, D. Fernández Del Val, J.P. Fernández Ramos, J. Flix, M.C. Fouz, O. Gonzalez Lopez, S. Goy Lopez, J.M. Hernandez, M.I. Josa, J. Llorente Merino, C. Martin Perez, E. Martin Viscasillas, D. Moran, C.M. Morcillo Perez, Á. Navarro Tobar, C. Perez Dengra, A. Pérez-Calero Yzquierdo, J. Puerta Pelayo, I. Redondo, J. Sastre, J. Vazquez Escobar



JHEP09(2025)141

**Universidad Autónoma de Madrid, Madrid, Spain**
J.F. de Trocóniz

**Universidad de Oviedo, Instituto Universitario de Ciencias y Tecnologías Espaciales de Asturias (ICTEA), Oviedo, Spain**
B. Alvarez Gonzalez, J. Cuevas, J. Fernandez Menendez, S. Folgueras, I. Gonzalez Caballero, P. Leguina, E. Palencia Cortezon, J. Prado Pico, V. Rodríguez Bouza, A. Soto Rodríguez, A. Trapote, C. Vico Villalba, P. Vischia

**Instituto de Física de Cantabria (IFCA), CSIC-Universidad de Cantabria, Santander, Spain**
S. Blanco Fernández, I.J. Cabrillo, A. Calderon, J. Duarte Campderros, M. Fernandez, G. Gomez, C. Lasaosa García, R. Lopez Ruiz, C. Martinez Rivero, P. Martinez Ruiz del Arbol, F. Matorras, P. Matorras Cuevas, E. Navarrete Ramos, J. Piedra Gomez, L. Scodellaro, I. Vila, J.M. Vizan Garcia

**University of Colombo, Colombo, Sri Lanka**
B. Kailasapathy[59], D.D.C. Wickramarathna

**University of Ruhuna, Department of Physics, Matara, Sri Lanka**
W.G.D. Dharmaratna[60], K. Liyanage, N. Perera

**CERN, European Organization for Nuclear Research, Geneva, Switzerland**
D. Abbaneo, C. Amendola, E. Auffray, J. Baechler, D. Barney, A. Bermúdez Martínez, M. Bianco, A.A. Bin Anuar, A. Bocci, L. Borgonovi, C. Botta, A. Bragagnolo, E. Brondolin, C.E. Brown, C. Caillol, G. Cerminara, N. Chernyavskaya, D. d'Enterria, A. Dabrowski, A. David, A. De Roeck, M.M. Defranchis, M. Deile, M. Dobson, G. Franzoni, W. Funk, S. Giani, D. Gigi, K. Gill, F. Glege, M. Glowacki, J. Hegeman, J.K. Heikkilä, B. Huber, V. Innocente, T. James, P. Janot, O. Kaluzinska, O. Karacheban[26], G. Karathanasis, S. Laurila, P. Lecoq, E. Leutgeb, C. Lourenço, M. Magherini, L. Malgeri, M. Mannelli, M. Matthewman, A. Mehta, F. Meijers, S. Mersi, E. Meschi, M. Migliorini, V. Milosevic, F. Monti, F. Moortgat, M. Mulders, I. Neutelings, S. Orfanelli, F. Pantaleo, G. Petrucciani, A. Pfeiffer, M. Pierini, M. Pitt, H. Qu, D. Rabady, B. Ribeiro Lopes, F. Riti, M. Rovere, H. Sakulin, R. Salvatico, S. Sanchez Cruz, S. Scarfi, C. Schwick, M. Selvaggi, A. Sharma, K. Shchelina, P. Silva, P. Sphicas[61], A.G. Stahl Leiton, A. Steen, S. Summers, D. Treille, P. Tropea, D. Walter, J. Wanczyk[62], J. Wang, S. Wuchterl, P. Zehetner, P. Zejdl, W.D. Zeuner

**PSI Center for Neutron and Muon Sciences, Villigen, Switzerland**
T. Bevilacqua[63], L. Caminada[63], A. Ebrahimi, W. Erdmann, R. Horisberger, Q. Ingram, H.C. Kaestli, D. Kotlinski, C. Lange, M. Missiroli[63], L. Noehte[63], T. Rohe, A. Samalan

**ETH Zurich - Institute for Particle Physics and Astrophysics (IPA), Zurich, Switzerland**
T.K. Aarrestad, M. Backhaus, G. Bonomelli, A. Calandri, C. Cazzaniga, K. Datta, P. De Bryas Dexmiers D'Archiac[62], A. De Cosa, G. Dissertori, M. Dittmar, M. Donegà,

F. Eble, M. Galli, K. Gedia, F. Glessgen, C. Grab, N. Härringer, T.G. Harte, D. Hits, W. Lustermann, A.-M. Lyon, R.A. Manzoni, M. Marchegiani, L. Marchese, A. Mascellani[62], F. Nessi-Tedaldi, F. Pauss, V. Perovic, S. Pigazzini, B. Ristic, R. Seidita, J. Steggemann[62], A. Tarabini, D. Valsecchi, R. Wallny

**Universität Zürich, Zurich, Switzerland**
C. Amsler[64], P. Bärtschi, M.F. Canelli, K. Cormier, M. Huwiler, W. Jin, A. Jofrehei, B. Kilminster, S. Leontsinis, S.P. Liechti, A. Macchiolo, P. Meiring, F. Meng, J. Motta, A. Reimers, P. Robmann, M. Senger, E. Shokr, F. Stäger, R. Tramontano

**National Central University, Chung-Li, Taiwan**
C. Adloff[65], D. Bhowmik, C.M. Kuo, W. Lin, P.K. Rout, P.C. Tiwari[36]

**National Taiwan University (NTU), Taipei, Taiwan**
L. Ceard, K.F. Chen, Z.g. Chen, A. De Iorio, W.-S. Hou, T.h. Hsu, Y.w. Kao, S. Karmakar, G. Kole, Y.y. Li, R.-S. Lu, E. Paganis, X.f. Su, J. Thomas-Wilsker, L.s. Tsai, D. Tsionou, H.y. Wu, E. Yazgan

**High Energy Physics Research Unit, Department of Physics, Faculty of Science, Chulalongkorn University, Bangkok, Thailand**
C. Asawatangtrakuldee, N. Srimanobhas, V. Wachirapusitanand

**Tunis El Manar University, Tunis, Tunisia**
Y. Maghrbi

**Çukurova University, Physics Department, Science and Art Faculty, Adana, Turkey**
D. Agyel, F. Boran, F. Dolek, I. Dumanoglu[66], E. Eskut, Y. Guler[67], E. Gurpinar Guler[67], C. Isik, O. Kara, A. Kayis Topaksu, Y. Komurcu, G. Onengut, K. Ozdemir[68], A. Polatoz, B. Tali[69], U.G. Tok, E. Uslan, I.S. Zorbakir

**Middle East Technical University, Physics Department, Ankara, Turkey**
M. Yalvac[70]

**Bogazici University, Istanbul, Turkey**
B. Akgun, I.O. Atakisi, E. Gülmez, M. Kaya[71], O. Kaya[72], S. Tekten[73]

**Istanbul Technical University, Istanbul, Turkey**
A. Cakir, K. Cankocak[66,74], S. Sen[75]

**Istanbul University, Istanbul, Turkey**
O. Aydilek[76], B. Hacisahinoglu, I. Hos[77], B. Kaynak, S. Ozkorucuklu, O. Potok, H. Sert, C. Simsek, C. Zorbilmez

**Yildiz Technical University, Istanbul, Turkey**
S. Cerci, B. Isildak[78], D. Sunar Cerci, T. Yetkin



JHEP09(2025)141

**Institute for Scintillation Materials of National Academy of Science of Ukraine, Kharkiv, Ukraine**

A. Boyaryntsev, B. Grynyov

**National Science Centre, Kharkiv Institute of Physics and Technology, Kharkiv, Ukraine**

L. Levchuk

**University of Bristol, Bristol, United Kingdom**

D. Anthony, J.J. Brooke, A. Bundock, F. Bury, E. Clement, D. Cussans, H. Flacher, J. Goldstein, H.F. Heath, M.-L. Holmberg, L. Kreczko, S. Paramesvaran, L. Robertshaw, V.J. Smith, K. Walkingshaw Pass

**Rutherford Appleton Laboratory, Didcot, United Kingdom**

A.H. Ball, K.W. Bell, A. Belyaev[79], C. Brew, R.M. Brown, D.J.A. Cockerill, C. Cooke, A. Elliot, K.V. Ellis, K. Harder, S. Harper, J. Linacre, K. Manolopoulos, D.M. Newbold, E. Olaiya, D. Petyt, T. Reis, A.R. Sahasransu, G. Salvi, T. Schuh, C.H. Shepherd-Themistocleous, I.R. Tomalin, K.C. Whalen, T. Williams

**Imperial College, London, United Kingdom**

I. Andreou, R. Bainbridge, P. Bloch, O. Buchmuller, C.A. Carrillo Montoya, G.S. Chahal[80], D. Colling, J.S. Dancu, I. Das, P. Dauncey, G. Davies, M. Della Negra, S. Fayer, G. Fedi, G. Hall, A. Howard, G. Iles, C.R. Knight, P. Krueper, J. Langford, K.H. Law, J. León Holgado, L. Lyons, A.-M. Magnan, B. Maier, S. Mallios, M. Mieskolainen, J. Nash[81], M. Pesaresi, P.B. Pradeep, B.C. Radburn-Smith, A. Richards, A. Rose, L. Russell, K. Savva, C. Seez, R. Shukla, A. Tapper, K. Uchida, G.P. Uttley, T. Virdee[28], M. Vojinovic, N. Wardle, D. Winterbottom

**Brunel University, Uxbridge, United Kingdom**

J.E. Cole, A. Khan, P. Kyberd, I.D. Reid

**Baylor University, Waco, Texas, USA**

S. Abdullin, A. Brinkerhoff, E. Collins, M.R. Darwish, J. Dittmann, K. Hatakeyama, V. Hegde, J. Hiltbrand, B. McMaster, J. Samudio, S. Sawant, C. Sutantawibul, J. Wilson

**Catholic University of America, Washington, DC, USA**

R. Bartek, A. Dominguez, A.E. Simsek, S.S. Yu

**The University of Alabama, Tuscaloosa, Alabama, USA**

B. Bam, A. Buchot Perraguin, R. Chudasama, S.I. Cooper, C. Crovella, S.V. Gleyzer, E. Pearson, C.U. Perez, P. Rumerio[82], E. Usai, R. Yi

**Boston University, Boston, Massachusetts, USA**

A. Akpinar, G. De Castro, Z. Demiragli, C. Erice, C. Fangmeier, C. Fernandez Madrazo, E. Fontanesi, D. Gastler, F. Golf, S. Jeon, J. O'Cain, I. Reed, J. Rohlf, K. Salyer, D. Sperka, D. Spitzbart, I. Suarez, A. Tsatsos, A.G. Zecchinelli



JHEP09(2025)141

**Brown University, Providence, Rhode Island, USA**

G. Barone, G. Benelli, D. Cutts, S. Ellis, L. Gouskos, M. Hadley, U. Heintz, K.W. Ho, J.M. Hogan[83], T. Kwon, G. Landsberg, K.T. Lau, J. Luo, S. Mondal, T. Russell, S. Sagir[84], X. Shen, M. Stamenkovic, N. Venkatasubramanian

**University of California, Davis, Davis, California, USA**

S. Abbott, B. Barton, C. Brainerd, R. Breedon, H. Cai, M. Calderon De La Barca Sanchez, M. Chertok, M. Citron, J. Conway, P.T. Cox, R. Erbacher, F. Jensen, O. Kukral, G. Mocellin, M. Mulhearn, S. Ostrom, W. Wei, S. Yoo, F. Zhang

**University of California, Los Angeles, California, USA**

K. Adamidis, M. Bachtis, D. Campos, R. Cousins, A. Datta, G. Flores Avila, J. Hauser, M. Ignatenko, M.A. Iqbal, T. Lam, Y.f. Lo, E. Manca, A. Nunez Del Prado, D. Saltzberg, V. Valuev

**University of California, Riverside, Riverside, California, USA**

R. Clare, J.W. Gary, G. Hanson

**University of California, San Diego, La Jolla, California, USA**

A. Aportela, A. Arora, J.G. Branson, S. Cittolin, S. Cooperstein, D. Diaz, J. Duarte, L. Giannini, Y. Gu, J. Guiang, R. Kansal, V. Krutelyov, R. Lee, J. Letts, M. Masciovecchio, F. Mokhtar, S. Mukherjee, M. Pieri, D. Primosch, M. Quinnan, V. Sharma, M. Tadel, E. Vourliotis, F. Würthwein, Y. Xiang, A. Yagil

**University of California, Santa Barbara - Department of Physics, Santa Barbara, California, USA**

A. Barzdukas, L. Brennan, C. Campagnari, K. Downham, C. Grieco, M.M. Hussain, J. Incandela, J. Kim, A.J. Li, P. Masterson, H. Mei, J. Richman, S.N. Santpur, U. Sarica, R. Schmitz, F. Setti, J. Sheplock, D. Stuart, T.Á. Vámi, X. Yan, D. Zhang

**California Institute of Technology, Pasadena, California, USA**

A. Albert, S. Bhattacharya, A. Bornheim, O. Cerri, J. Mao, H.B. Newman, G. Reales Gutiérrez, M. Spiropulu, J.R. Vlimant, S. Xie, R.Y. Zhu

**Carnegie Mellon University, Pittsburgh, Pennsylvania, USA**

J. Alison, S. An, P. Bryant, M. Cremonesi, V. Dutta, T. Ferguson, T.A. Gómez Espinosa, A. Harilal, A. Kallil Tharayil, M. Kanemura, C. Liu, T. Mudholkar, S. Murthy, P. Palit, K. Park, M. Paulini, A. Roberts, A. Sanchez, W. Terrill

**University of Colorado Boulder, Boulder, Colorado, USA**

J.P. Cumalat, W.T. Ford, A. Hart, A. Hassani, N. Manganelli, J. Pearkes, C. Savard, N. Schonbeck, K. Stenson, K.A. Ulmer, S.R. Wagner, N. Zipper, D. Zuolo




JHEP09(2025)141

**Cornell University, Ithaca, New York, USA**

J. Alexander, X. Chen, D.J. Cranshaw, J. Dickinson, J. Fan, X. Fan, J. Grassi, S. Hogan, P. Kotamnives, J. Monroy, G. Niendorf, M. Oshiro, J.R. Patterson, M. Reid, A. Ryd, J. Thom, P. Wittich, R. Zou

**Fermi National Accelerator Laboratory, Batavia, Illinois, USA**

M. Albrow, M. Alyari, O. Amram, G. Apollinari, A. Apresyan, L.A.T. Bauerdick, D. Berry, J. Berryhill, P.C. Bhat, K. Burkett, J.N. Butler, A. Canepa, G.B. Cerati, H.W.K. Cheung, F. Chlebana, C. Cosby, G. Cummings, I. Dutta, V.D. Elvira, J. Freeman, A. Gandrakota, Z. Gecse, L. Gray, D. Green, A. Grummer, S. Grünendahl, D. Guerrero, O. Gutsche, R.M. Harris, T.C. Herwig, J. Hirschauer, B. Jayatilaka, S. Jindariani, M. Johnson, U. Joshi, T. Klijnsma, B. Klima, K.H.M. Kwok, S. Lammel, C. Lee, D. Lincoln, R. Lipton, T. Liu, K. Maeshima, D. Mason, P. McBride, P. Merkel, S. Mrenna, S. Nahn, J. Ngadiuba, D. Noonan, S. Norberg, V. Papadimitriou, N. Pastika, K. Pedro, C. Pena[85], F. Ravera, A. Reinsvold Hall[86], L. Ristori, M. Safdari, E. Sexton-Kennedy, N. Smith, A. Soha, L. Spiegel, S. Stoynev, J. Strait, L. Taylor, S. Tkaczyk, N.V. Tran, L. Uplegger, E.W. Vaandering, C. Wang, I. Zoi

**University of Florida, Gainesville, Florida, USA**

C. Aruta, P. Avery, D. Bourilkov, P. Chang, V. Cherepanov, R.D. Field, C. Huh, E. Koenig, M. Kolosova, J. Konigsberg, A. Korytov, K. Matchev, N. Menendez, G. Mitselmakher, K. Mohrman, A. Muthirakalayil Madhu, N. Rawal, S. Rosenzweig, Y. Takahashi, J. Wang

**Florida State University, Tallahassee, Florida, USA**

T. Adams, A. Al Kadhim, A. Askew, S. Bower, R. Hashmi, R.S. Kim, S. Kim, T. Kolberg, G. Martinez, H. Prosper, P.R. Prova, M. Wulansatiti, R. Yohay, J. Zhang

**Florida Institute of Technology, Melbourne, Florida, USA**

B. Alsufyani, S. Butalla, S. Das, T. Elkafrawy[17], M. Hohlmann, E. Yanes

**University of Illinois Chicago, Chicago, Illinois, USA**

M.R. Adams, A. Baty, C. Bennett, R. Cavanaugh, R. Escobar Franco, O. Evdokimov, C.E. Gerber, H. Gupta, M. Hawksworth, A. Hingrajiya, D.J. Hofman, J.h. Lee, D.S. Lemos, C. Mills, S. Nanda, G. Oh, B. Ozek, D. Pilipovic, R. Pradhan, E. Prifti, P. Roy, T. Roy, S. Rudrabhatla, N. Singh, M.B. Tonjes, N. Varelas, M.A. Wadud, Z. Ye, J. Yoo

**The University of Iowa, Iowa City, Iowa, USA**

M. Alhusseini, D. Blend, K. Dilsiz[87], L. Emediato, G. Karaman, O.K. Köseyan, J.-P. Merlo, A. Mestvirishvili[88], O. Neogi, H. Ogul[89], Y. Onel, A. Penzo, C. Snyder, E. Tiras[90]

**Johns Hopkins University, Baltimore, Maryland, USA**
B. Blumenfeld, L. Corcodilos, J. Davis, A.V. Gritsan, L. Kang, S. Kyriacou, P. Maksimovic, M. Roguljic, J. Roskes, S. Sekhar, M. Swartz

**The University of Kansas, Lawrence, Kansas, USA**
A. Abreu, L.F. Alcerro Alcerro, J. Anguiano, S. Arteaga Escatel, P. Baringer, A. Bean, Z. Flowers, D. Grove, J. King, G. Krintiras, M. Lazarovits, C. Le Mahieu, J. Marquez, M. Murray, M. Nickel, S. Popescu[91], C. Rogan, C. Royon, S. Sanders, C. Smith, G. Wilson

**Kansas State University, Manhattan, Kansas, USA**
B. Allmond, R. Gujju Gurunadha, A. Ivanov, K. Kaadze, Y. Maravin, J. Natoli, D. Roy, G. Sorrentino

**University of Maryland, College Park, Maryland, USA**
A. Baden, A. Belloni, J. Bistany-riebman, S.C. Eno, N.J. Hadley, S. Jabeen, R.G. Kellogg, T. Koeth, B. Kronheim, S. Lascio, P. Major, A.C. Mignerey, S. Nabili, C. Palmer, C. Papageorgakis, M.M. Paranjpe, E. Popova[92], A. Shevelev, L. Wang, L. Zhang

**Massachusetts Institute of Technology, Cambridge, Massachusetts, USA**
C. Baldenegro Barrera, J. Bendavid, S. Bright-Thonney, I.A. Cali, P.c. Chou, M. D'Alfonso, J. Eysermans, C. Freer, G. Gomez-Ceballos, M. Goncharov, G. Grosso, P. Harris, D. Hoang, D. Kovalskyi, J. Krupa, L. Lavezzo, Y.-J. Lee, K. Long, C. Mcginn, A. Novak, M.I. Park, C. Paus, C. Reissel, C. Roland, G. Roland, S. Rothman, G.S.F. Stephans, Z. Wang, B. Wyslouch, T.J. Yang

**University of Minnesota, Minneapolis, Minnesota, USA**
B. Crossman, C. Kapsiak, M. Krohn, D. Mahon, J. Mans, B. Marzocchi, M. Revering, R. Rusack, R. Saradhy, N. Strobbe

**University of Nebraska-Lincoln, Lincoln, Nebraska, USA**
K. Bloom, D.R. Claes, G. Haza, J. Hossain, C. Joo, I. Kravchenko, A. Rohilla, J.E. Siado, W. Tabb, A. Vagnerini, A. Wightman, F. Yan, D. Yu

**State University of New York at Buffalo, Buffalo, New York, USA**
H. Bandyopadhyay, L. Hay, H.w. Hsia, I. Iashvili, A. Kalogeropoulos, A. Kharchilava, M. Morris, D. Nguyen, S. Rappoccio, H. Rejeb Sfar, A. Williams, P. Young

**Northeastern University, Boston, Massachusetts, USA**
G. Alverson, E. Barberis, J. Bonilla, B. Bylsma, M. Campana, J. Dervan, Y. Haddad, Y. Han, I. Israr, A. Krishna, P. Levchenko, J. Li, M. Lu, R. Mccarthy, D.M. Morse, T. Orimoto, A. Parker, L. Skinnari, E. Tsai, D. Wood

**Northwestern University, Evanston, Illinois, USA**
S. Dittmer, K.A. Hahn, D. Li, Y. Liu, M. Mcginnis, Y. Miao, D.G. Monk, M.H. Schmitt, A. Taliercio, M. Velasco



JHEP09(2025)141

**University of Notre Dame, Notre Dame, Indiana, USA**

G. Agarwal, R. Band, R. Bucci, S. Castells, A. Das, R. Goldouzian, M. Hildreth, K. Hurtado Anampa, T. Ivanov, C. Jessop, K. Lannon, J. Lawrence, N. Loukas, L. Lutton, J. Mariano, N. Marinelli, I. Mcalister, T. McCauley, C. Mcgrady, C. Moore, Y. Musienko[21], H. Nelson, M. Osherson, A. Piccinelli, R. Ruchti, A. Townsend, Y. Wan, M. Wayne, H. Yockey, M. Zarucki, L. Zygala

**The Ohio State University, Columbus, Ohio, USA**

A. Basnet, M. Carrigan, L.S. Durkin, C. Hill, M. Joyce, M. Nunez Ornelas, K. Wei, D.A. Wenzl, B.L. Winer, B.R. Yates

**Princeton University, Princeton, New Jersey, USA**

H. Bouchamaoui, K. Coldham, P. Das, G. Dezoort, P. Elmer, P. Fackeldey, A. Frankenthal, B. Greenberg, N. Haubrich, K. Kennedy, G. Kopp, S. Kwan, Y. Lai, D. Lange, A. Loeliger, D. Marlow, I. Ojalvo, J. Olsen, F. Simpson, D. Stickland, C. Tully, L.H. Vage

**University of Puerto Rico, Mayaguez, Puerto Rico, USA**

S. Malik, R. Sharma

**Purdue University, West Lafayette, Indiana, USA**

A.S. Bakshi, S. Chandra, R. Chawla, A. Gu, L. Gutay, M. Jones, A.W. Jung, A.M. Koshy, M. Liu, G. Negro, N. Neumeister, G. Paspalaki, S. Piperov, J.F. Schulte, A.K. Virdi, F. Wang, A. Wildridge, W. Xie, Y. Yao

**Purdue University Northwest, Hammond, Indiana, USA**

J. Dolen, N. Parashar, A. Pathak

**Rice University, Houston, Texas, USA**

D. Acosta, A. Agrawal, T. Carnahan, K.M. Ecklund, P.J. Fernández Manteca, S. Freed, P. Gardner, F.J.M. Geurts, I. Krommydas, W. Li, J. Lin, O. Miguel Colin, B.P. Padley, R. Redjimi, J. Rotter, E. Yigitbasi, Y. Zhang

**University of Rochester, Rochester, New York, USA**

A. Bodek, P. de Barbaro, R. Demina, J.L. Dulemba, A. Garcia-Bellido, O. Hindrichs, A. Khukhunaishvili, N. Parmar, P. Parygin[92], R. Taus

**Rutgers, The State University of New Jersey, Piscataway, New Jersey, USA**

B. Chiarito, J.P. Chou, S.V. Clark, D. Gadkari, Y. Gershtein, E. Halkiadakis, M. Heindl, C. Houghton, D. Jaroslawski, S. Konstantinou, I. Laflotte, A. Lath, J. Martins, R. Montalvo, K. Nash, J. Reichert, P. Saha, S. Salur, S. Schnetzer, S. Somalwar, R. Stone, S.A. Thayil, S. Thomas, J. Vora

**University of Tennessee, Knoxville, Tennessee, USA**

D. Ally, A.G. Delannoy, S. Fiorendi, S. Higginbotham, T. Holmes, A.R. Kanuganti, N. Karunarathna, L. Lee, E. Nibigira, S. Spanier



JHEP09(2025)141

**Texas A&M University, College Station, Texas, USA**
D. Aebi, M. Ahmad, T. Akhter, K. Androsov[62], O. Bouhali[93], R. Eusebi, J. Gilmore, T. Huang, T. Kamon[94], H. Kim, S. Luo, R. Mueller, D. Overton, A. Safonov

**Texas Tech University, Lubbock, Texas, USA**
N. Akchurin, J. Damgov, Y. Feng, N. Gogate, Y. Kazhykarim, K. Lamichhane, S.W. Lee, C. Madrid, A. Mankel, T. Peltola, I. Volobouev

**Vanderbilt University, Nashville, Tennessee, USA**
E. Appelt, Y. Chen, S. Greene, A. Gurrola, W. Johns, R. Kunnawalkam Elayavalli, A. Melo, D. Rathjens, F. Romeo, P. Sheldon, S. Tuo, J. Velkovska, J. Viinikainen

**University of Virginia, Charlottesville, Virginia, USA**
B. Cardwell, H. Chung, B. Cox, J. Hakala, R. Hirosky, A. Ledovskoy, C. Mantilla, C. Neu, C. Ramón Álvarez

**Wayne State University, Detroit, Michigan, USA**
S. Bhattacharya, P.E. Karchin

**University of Wisconsin - Madison, Madison, Wisconsin, USA**
A. Aravind, S. Banerjee, K. Black, T. Bose, E. Chavez, S. Dasu, P. Everaerts, C. Galloni, H. He, M. Herndon, A. Herve, C.K. Koraka, A. Lanaro, R. Loveless, J. Madhusudanan Sreekala, A. Mallampalli, A. Mohammadi, S. Mondal, G. Parida, L. Pétré, D. Pinna, A. Savin, V. Shang, V. Sharma, W.H. Smith, D. Teague, H.F. Tsoi, W. Vetens, A. Warden

**Authors affiliated with an international laboratory covered by a cooperation agreement with CERN**
G. Gavrilov, V. Golovtcov, Y. Ivanov, V. Kim[95], V. Murzin, V. Oreshkin, D. Sosnov, V. Sulimov, L. Uvarov, A. Vorobyev[†]

**Authors affiliated with an institute formerly covered by a cooperation agreement with CERN**
S. Afanasiev, V. Alexakhin, Yu. Andreev, T. Aushev, D. Budkouski, A. Ershov[95], I. Golutvin[†], I. Gorbunov, V. Karjavine, V. Klyukhin[95], O. Kodolova[96,92], V. Korenkov, A. Lanev, A. Malakhov, V. Matveev[95], A. Nikitenko[97,96], V. Palichik, V. Perelygin, S. Petrushanko[95], M. Savina, V. Shalaev, S. Shmatov, S. Shulha, V. Smirnov, O. Teryaev, A. Toropin, N. Voytishin, B.S. Yuldashev[†,98], A. Zarubin, I. Zhizhin, A. Dermenev, S. Gninenko, N. Golubev, A. Karneyeu, D. Kirpichnikov, M. Kirsanov, N. Krasnikov, I. Tlisova, K. Ivanov, V. Gavrilov, N. Lychkovskaya, V. Popov, A. Zhokin, R. Chistov[95], M. Danilov[95], S. Polikarpov[95], V. Andreev, M. Azarkin, M. Kirakosyan, A. Terkulov, E. Boos, V. Bunichev, M. Dubinin[85], L. Dudko, A. Gribushin, M. Perfilov, V. Savrin, V. Blinov[95], T. Dimova[95], A. Kozyrev[95], O. Radchenko[95], Y. Skovpen[95], V. Kachanov, S. Slabospitskii, A. Uzunian, A. Babaev, V. Borshch, D. Druzhkin



JHEP09(2025)141

[†] *Deceased*
[1] *Also at Yerevan State University, Yerevan, Armenia*
[2] *Also at TU Wien, Vienna, Austria*
[3] *Also at Ghent University, Ghent, Belgium*
[4] *Also at Universidade do Estado do Rio de Janeiro, Rio de Janeiro, Brazil*
[5] *Also at FACAMP - Faculdades de Campinas, Sao Paulo, Brazil*
[6] *Also at Universidade Estadual de Campinas, Campinas, Brazil*
[7] *Also at Federal University of Rio Grande do Sul, Porto Alegre, Brazil*
[8] *Also at University of Chinese Academy of Sciences, Beijing, China*
[9] *Also at China Center of Advanced Science and Technology, Beijing, China*
[10] *Also at University of Chinese Academy of Sciences, Beijing, China*
[11] *Also at China Spallation Neutron Source, Guangdong, China*
[12] *Now at Henan Normal University, Xinxiang, China*
[13] *Also at University of Shanghai for Science and Technology, Shanghai, China*
[14] *Now at The University of Iowa, Iowa City, Iowa, USA*
[15] *Also at Zewail City of Science and Technology, Zewail, Egypt*
[16] *Also at British University in Egypt, Cairo, Egypt*
[17] *Now at Ain Shams University, Cairo, Egypt*
[18] *Also at Purdue University, West Lafayette, Indiana, USA*
[19] *Also at Université de Haute Alsace, Mulhouse, France*
[20] *Also at Istinye University, Istanbul, Turkey*
[21] *Also at an institute formerly covered by a cooperation agreement with CERN*
[22] *Also at The University of the State of Amazonas, Manaus, Brazil*
[23] *Also at University of Hamburg, Hamburg, Germany*
[24] *Also at RWTH Aachen University, III. Physikalisches Institut A, Aachen, Germany*
[25] *Also at Bergische University Wuppertal (BUW), Wuppertal, Germany*
[26] *Also at Brandenburg University of Technology, Cottbus, Germany*
[27] *Also at Forschungszentrum Jülich, Juelich, Germany*
[28] *Also at CERN, European Organization for Nuclear Research, Geneva, Switzerland*
[29] *Also at HUN-REN ATOMKI - Institute of Nuclear Research, Debrecen, Hungary*
[30] *Now at Universitatea Babes-Bolyai - Facultatea de Fizica, Cluj-Napoca, Romania*
[31] *Also at MTA-ELTE Lendület CMS Particle and Nuclear Physics Group, Eötvös Loránd University, Budapest, Hungary*
[32] *Also at HUN-REN Wigner Research Centre for Physics, Budapest, Hungary*
[33] *Also at Physics Department, Faculty of Science, Assiut University, Assiut, Egypt*
[34] *Also at Punjab Agricultural University, Ludhiana, India*
[35] *Also at University of Visva-Bharati, Santiniketan, India*
[36] *Also at Indian Institute of Science (IISc), Bangalore, India*
[37] *Also at Amity University Uttar Pradesh, Noida, India*
[38] *Also at UPES - University of Petroleum and Energy Studies, Dehradun, India*
[39] *Also at IIT Bhubaneswar, Bhubaneswar, India*
[40] *Also at Institute of Physics, Bhubaneswar, India*
[41] *Also at University of Hyderabad, Hyderabad, India*
[42] *Also at Department of Physics, Isfahan University of Technology, Isfahan, Iran*
[43] *Also at Sharif University of Technology, Tehran, Iran*
[44] *Also at Department of Physics, University of Science and Technology of Mazandaran, Behshahr, Iran*
[45] *Also at Department of Physics, Faculty of Science, Arak University, ARAK, Iran*
[46] *Also at Helwan University, Cairo, Egypt*
[47] *Also at Italian National Agency for New Technologies, Energy and Sustainable Economic Development, Bologna, Italy*
[48] *Also at Centro Siciliano di Fisica Nucleare e di Struttura Della Materia, Catania, Italy*
[49] *Also at Università degli Studi Guglielmo Marconi, Roma, Italy*
[50] *Also at Scuola Superiore Meridionale, Università di Napoli 'Federico II', Napoli, Italy*
[51] *Also at Fermi National Accelerator Laboratory, Batavia, Illinois, USA*

[52] *Also at Laboratori Nazionali di Legnaro dell'INFN, Legnaro, Italy*
[53] *Also at Lulea University of Technology, Lulea, Sweden*
[54] *Also at Consiglio Nazionale delle Ricerche - Istituto Officina dei Materiali, Perugia, Italy*
[55] *Also at Institut de Physique des 2 Infinis de Lyon (IP2I), Villeurbanne, France*
[56] *Also at Department of Applied Physics, Faculty of Science and Technology, Universiti Kebangsaan Malaysia, Bangi, Malaysia*
[57] *Also at Consejo Nacional de Ciencia y Tecnología, Mexico City, Mexico*
[58] *Also at INFN Sezione di Torino, Università di Torino, Torino, Italy; Università del Piemonte Orientale, Novara, Italy*
[59] *Also at Trincomalee Campus, Eastern University, Sri Lanka, Nilaveli, Sri Lanka*
[60] *Also at Saegis Campus, Nugegoda, Sri Lanka*
[61] *Also at National and Kapodistrian University of Athens, Athens, Greece*
[62] *Also at Ecole Polytechnique Fédérale Lausanne, Lausanne, Switzerland*
[63] *Also at Universität Zürich, Zurich, Switzerland*
[64] *Also at Stefan Meyer Institute for Subatomic Physics, Vienna, Austria*
[65] *Also at Laboratoire d'Annecy-le-Vieux de Physique des Particules, IN2P3-CNRS, Annecy-le-Vieux, France*
[66] *Also at Near East University, Research Center of Experimental Health Science, Mersin, Turkey*
[67] *Also at Konya Technical University, Konya, Turkey*
[68] *Also at Izmir Bakircay University, Izmir, Turkey*
[69] *Also at Adiyaman University, Adiyaman, Turkey*
[70] *Also at Bozok Universitetesi Rektörlügü, Yozgat, Turkey*
[71] *Also at Marmara University, Istanbul, Turkey*
[72] *Also at Milli Savunma University, Istanbul, Turkey*
[73] *Also at Kafkas University, Kars, Turkey*
[74] *Now at Istanbul Okan University, Istanbul, Turkey*
[75] *Also at Hacettepe University, Ankara, Turkey*
[76] *Also at Erzincan Binali Yildirim University, Erzincan, Turkey*
[77] *Also at Istanbul University - Cerrahpasa, Faculty of Engineering, Istanbul, Turkey*
[78] *Also at Yildiz Technical University, Istanbul, Turkey*
[79] *Also at School of Physics and Astronomy, University of Southampton, Southampton, United Kingdom*
[80] *Also at IPPP Durham University, Durham, United Kingdom*
[81] *Also at Monash University, Faculty of Science, Clayton, Australia*
[82] *Also at Università di Torino, Torino, Italy*
[83] *Also at Bethel University, St. Paul, Minnesota, USA*
[84] *Also at Karamanoğlu Mehmetbey University, Karaman, Turkey*
[85] *Also at California Institute of Technology, Pasadena, California, USA*
[86] *Also at United States Naval Academy, Annapolis, Maryland, USA*
[87] *Also at Bingol University, Bingol, Turkey*
[88] *Also at Georgian Technical University, Tbilisi, Georgia*
[89] *Also at Sinop University, Sinop, Turkey*
[90] *Also at Erciyes University, Kayseri, Turkey*
[91] *Also at Horia Hulubei National Institute of Physics and Nuclear Engineering (IFIN-HH), Bucharest, Romania*
[92] *Now at another institute formerly covered by a cooperation agreement with CERN*
[93] *Also at Texas A&M University at Qatar, Doha, Qatar*
[94] *Also at Kyungpook National University, Daegu, Korea*
[95] *Also at another institute formerly covered by a cooperation agreement with CERN*
[96] *Also at Yerevan Physics Institute, Yerevan, Armenia*
[97] *Also at Imperial College, London, United Kingdom*
[98] *Also at Institute of Nuclear Physics of the Uzbekistan Academy of Sciences, Tashkent, Uzbekistan*

JHEP09(2025)141